CORRUGATED AND UNIFORM DIELECTRIC ROD AERIAL EXCITED IN E_0-MODE

By K. N. SHANKARA AND S. K. CHATTERJEE
(*Indian Institute of Science, Bangalore-12*)

[Received : February 10, 1972]

1. ABSTRACT

Expressions for the radiation pattern and gain of uniform and corrugated dielectric rod aerial excited in E_0-mode have been derived. The position, and number of lobes, beam width and relative magnitudes of lobes are fuuctions of the spacing and depth of grooves. The radiation characteristics also depend on length, diameter and dielectric constant of the aerial.

2. INTRODUCTION

The present work is a part of the programme of investigations[1-8] on dielectric and dielectric coated aerials of different shapes and of differently modified surface which are being conducted for the last two decades. Several other authors[9-20] have also made significant contributions in the field of dielectric aerials.

3. RADIATION FROM UNIFORM DIELECTRIC ROD

The radiation pattern has been derived by first considering radiation to take place from only the surface of the rod (Case A) and then the general relation has been derived by considering radiation to take place from both the surface as well as the end (Case B).

3.1 *Field Components*

The expressions for the field components of a uniform dielectric rod excited in E_0-mode are,

For $\rho \leqslant a$

$$E_{\rho 1} = [B k'_1 \beta / \omega \epsilon_1] \, J_1 (k'_1 \rho) \exp(-j \beta z)$$

$$E_{z1} = [B (k'_1)^2 / j \omega \epsilon_1] \, J_0 (k'_1 \rho) \exp(-j \beta z)$$

$$H'_{\phi 1} = B k'_1 \, J_1 (k'_1 \rho) \exp(-j \beta z) \qquad [1]$$

* The project is supported by PL-480 contract No. E-262-69(N), dated June 15, 1969.

3.2 *Transformation of Co-ordinates*

A transformation from (ρ, ϕ', z) system to spherical (r, ϕ, z) co-ordinate system is given by (See Fig. 1)

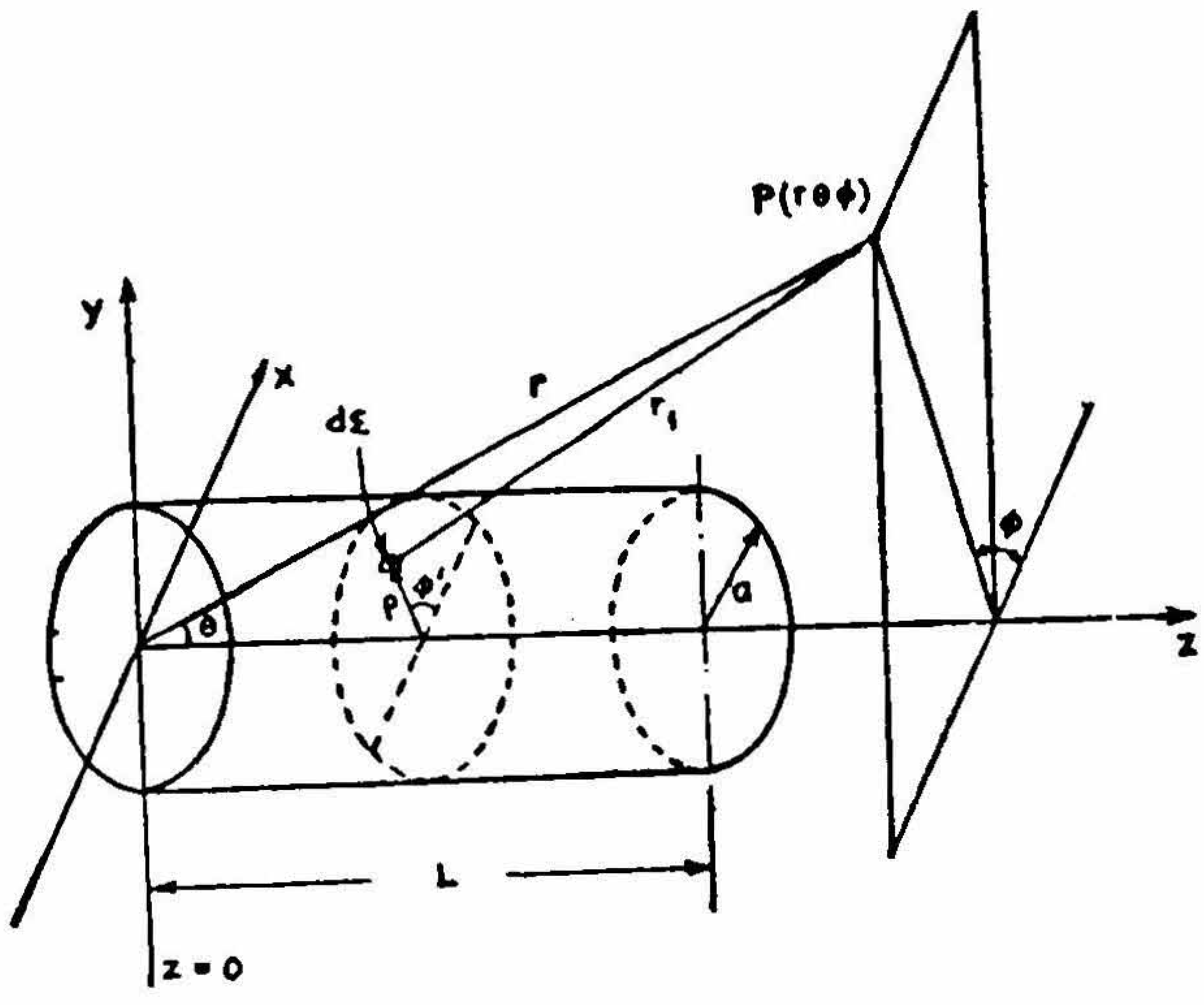

FIG. 1

Co ordinate system used in pattern computation (Case A)

L = Length of the rod $d\Sigma$ = Elemental surface considered
a = Radius of the rod ($r\ \theta\ \phi$) = Spherical co-ordinates
($\rho\ \phi'\ z$) = Circular cylindrical co-orcinates

TABLE 1

Transformation of Co-ordinates

	r	$\vec{\theta}$	$\vec{\phi}$
$\vec{\rho}$	$\sin\theta\cos(\phi'-\phi)$	$\cos\theta$ eos $(\phi'-\phi)$	$\sin(\phi'-\phi)$
$\vec{\phi}$	$-\sin\theta\sin(\phi'-\phi)$	$-\cos\theta\sin(\phi'-\phi)$	$\cos(\phi'-\phi)$
z	$\cos\theta$	$-\sin\theta$	0

3.3 *Evaluation of the Radiation Field.*

Case A : Radiation from the surface.

The electric and magnetic fields $\mathbf{E}_p$ and $\mathbf{H}_p$ respectively at the distant point $P(r, \theta, \phi)$ (see Fig. 1) are given in terms of the magnetic and vector potentials A^H and A^E respectively by the following relations

$$\mathbf{E}_p = -j\omega\epsilon_0 \mathbf{A}^H + \frac{1}{j\omega\epsilon_0} \text{grad div } \mathbf{A}^H - \text{curl } \mathbf{A}^E$$

$$\mathbf{H}_p = -j\omega\epsilon_0 \mathbf{A}^H + \frac{1}{j\omega\epsilon_0} \text{grad div } \mathbf{A}^E + \text{eur l } \mathbf{A}^H \quad [2]$$

where, A^E and A^H are given as

$$\mathbf{A}^E = \frac{1}{4\pi} \iint_\Sigma \mathbf{M} \frac{\exp j(\omega t - k r_1)}{r_1} d\Sigma$$

$$A^H = \frac{1}{4\pi} \iint_\Sigma \mathbf{J} \frac{\exp j(\omega t - k r_1)}{r_1} d\Sigma \quad [3]$$

where,

$$r_1 = r - a \sin\theta \cos(\phi' - \phi) - z \cos\theta \quad [4]$$

r = distance between $P(r, \theta, \phi)$ and the origin

$\mathbf{J} = \mathbf{n} \times \mathbf{H}$

$\mathbf{M} = -\mathbf{n} \times \mathbf{E}$ [5]

$\mathbf{n}$ = unit normal vector directed outside the surface

E, H represent the values of the electric and magnetic field vectors on the surface. **J, M** = Sheet electric and magnetic currents over the surface $k = 2\pi/\lambda_0$, the free space wave number. A time dependance of $\exp(j\omega t)$, is assumed.

$$\mathbf{J} = \vec{\rho} \times \vec{\phi}' \; \mathrm{H}_{\phi'} = \mathbf{z} \; \mathrm{H}_{\phi'} = \mathbf{z} \; C_3 \exp(-j\beta z) \quad [6]$$

$$\mathbf{M} = -\vec{\rho} \times \mathbf{z} \; E_z = \vec{\phi}' \; E_z = \vec{\phi}' \; C_2 \exp(-j\beta z) \quad [7]$$

where,

$$C_2 = \frac{B(k'_1)^2}{j\omega\epsilon_1} \mathrm{J}_0(k'_1 a) \quad [8]$$

$$C_3 = B k'_1 \mathrm{J}(k'_1 a) \quad [9]$$

Transforming J and M into spherical polar coordinates (see Table 1).

$$\mathbf{J} = C_3 [\mathbf{r} \cos\theta - \theta \sin\theta + \phi (0)] \exp(-j\beta z)$$

$$\mathbf{M} = C_3 [-\mathbf{r} \sin\theta \sin(\phi' - \vec{\phi}) - \vec{\theta} \cos\theta \sin(\phi' - \phi) + \vec{\phi} \cos(\phi' - \phi)] \exp(-j\beta z) \quad [10]$$

If $d\mathbf{A}^H$ and $d\mathbf{A}^E$ are the vector potentials at $P(r, \theta, \phi)$ due to the surface element $d\Sigma$ $(= a\, d\phi'\, d z)$. then the vector potentials A^H and A^E due to the complete surface of the rod are

$$\mathbf{A}^H = \int_{z=0}^{L} \int_{\phi'=0}^{2\pi} d\,A^H = \int_{z=0}^{L} \int_{\phi'=0}^{2\pi} \frac{\mathbf{J} \exp j(\omega t - k r_1)}{4\pi r_1} d\Sigma \quad [11]$$

and

$$\mathbf{A}^E = \int_{z=0}^{L} \int_{\phi'=0}^{2\pi} \frac{\mathbf{M} \exp j(\omega t - k r_1)}{4\pi r_1} d\Sigma \quad [12]$$

where, L is the length of the dielectric rod. The electric field at P is

$$\mathbf{E}_p = \int_{z=0}^{L} \int_{\phi'=0}^{2\pi} \left(-j\omega \mu_0\, d\,\mathbf{A}^H + \frac{1}{j\omega\epsilon_0} \text{grad div } d\,\mathbf{A}^H - \text{curl } d\,\mathbf{A}^E \right) d\Sigma \quad [13]$$

By transforming the vector operators into spherical polar co-ordinates, replacing r by r_1 in the denominator of the expression for $\mathbf{E}_p$ obtained after vector operations and neglecting terms containing higher powers of $1/r_1$, equation 13 reduces to

$$E_{PS} = \left[\left(\frac{-j\,a}{4\pi r} \exp(j\omega t - jkr) \right) \left\{ \int_0^L \exp -j(\beta z - kz\cos\theta) \right\} dz \right] \times$$

$$\left[\left\{ \vec{\theta} \int_0^{2\pi} \omega\mu_0 (-\sin\theta)\, C_3 \exp(j u \cos(\phi' - \phi)\, d\phi' \right\} \right.$$

$$+ \left\{ \vec{\theta} \int_0^{2\pi} k\, C_2 \cos(\phi' - \phi) \exp(j u \cos(\phi' - \phi)\, d\phi' \right\}$$

$$\left. + \left\{ \vec{\theta} \int_0^{2\pi} k\, C_2 \cos\theta \sin((\phi' - \phi) \exp(j u \cos(\phi' - \phi)) \right\} d\phi' \right] \quad [14]$$

which yields

$$\mathbf{E}_{PS} = \left(B \frac{j}{2r} (\mu_0/\epsilon_0)^{1/2} \, k \, k'_1 \, L \, a \, J_1(k'_1 a) \right) \times \left(\exp j(\omega t - kr) \exp \left\{ -j \frac{L}{2} (\beta - k \cos \theta) \right\} \right) \times \left(\frac{\sin x}{x} \{ J_0(k a \sin \theta) \sin \theta - C J_1(k a \sin \theta) \} \right) \qquad [15]$$

where,

$$x = \frac{L}{2} (\beta - k \cos \theta) \qquad [15a]$$

$$C = \frac{k'_1 \, J_0(k'_1 a)}{r_1 \, k \, J_1(k'_1 a)} \qquad [15b]$$

Case A': Free End Radiation.

The equivalent electric and magnetic current sheets are (See Fig. 2)

$$\mathbf{J} = \mathbf{z} \times \vec{\phi}' \, H_{\phi'} = -\vec{\rho} \, H_{\phi'} = \vec{\rho} \, D_1 \, J_1(k'_1 \rho) \qquad [16]$$

and

$$\mathbf{M} = -\mathbf{Z} \times \vec{\rho} \, E_\rho = -\vec{\phi}' \, E_\rho = \vec{\phi}' \, D_2 \, J_1(k'_1 \rho) \qquad [17]$$

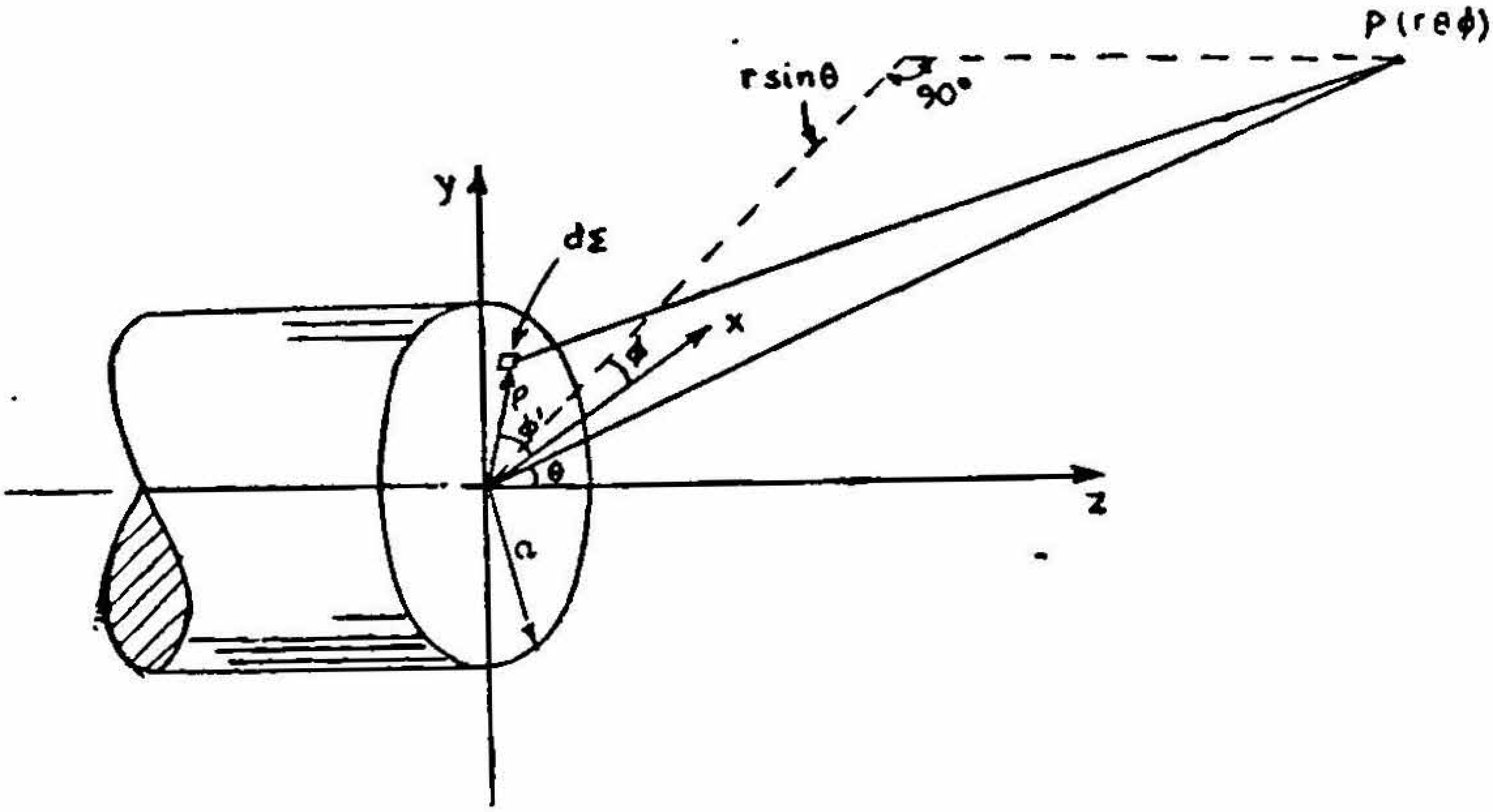

FIG. 2

Co-ordinate system used in pattern computation (Case A′)

a = Radius of the rod $(r\ \theta\ \phi)$ = Spherical co ordinates

$(\rho\ \phi'\ z)$ = Circular cylindrical co-ordinates where, $D_1 = -B\, k'_1$ [16a]

$$D_2 = -\frac{\beta\, B\, k'_1}{\omega \epsilon_1}$$ [17a]

By co-ordinate transformation equations [16] and]17] become

$$\mathbf{J} = D_1\, J_1(k'_1 \rho)\, [\mathbf{r} \sin\theta \cos(\phi' - \phi) + \vec{\theta} \cos\theta \cos(\phi' - \theta) + \vec{\phi} \sin(\phi' - \phi)] \quad [18]$$

$$M = D_2\, J_1(k'_1 \rho)\, [-\mathbf{r} \sin\theta \sin(\phi' - \phi) - \vec{\theta} \cos\theta \sin(\phi' - \phi) + \vec{\phi} \cos(\phi' - \phi)] \quad [19]$$

where,

$$r_1 = r - \rho \sin\theta \cos(\phi' - \phi) \quad \text{and} \quad d\Sigma = \rho\, d\rho\, d\phi'$$

The field at P due to radiation from the end of the rod is

$$\mathbf{E}_{pc} = \left(\frac{-j \exp j(\omega t - kr)}{4\pi r}\right) \int_{\rho=0}^{a} \int_{\phi'=0}^{2\pi} [\vec{\theta}(\omega \mu_0 \mathbf{J}_\theta + k\, \mathbf{M}_\phi) + \phi'(\omega \mu_0 \mathbf{J}_\phi - k\, \mathbf{M}_\theta)]$$
$$\times [\exp\{jk\rho \sin\theta \cos(\phi' - \phi)\}\, d\rho\, d\phi']$$

which reduces to

$$\mathbf{E}_{pe} = \left(\frac{B(\mu_0/\epsilon_0)^{1/2}\, k\, k'_1\, a\, J_1(k'_1 a)}{2\, r} \exp j(\omega t - kr)\right)$$
$$\left[\left(k \cos\theta + \frac{\beta}{\epsilon r_1}\right)\left(\frac{J_0(ka \sin\theta) \sin\theta - D\epsilon_{r1}\, J_1(ka \sin\theta)}{(k'_1)^2 - (k \sin\theta)^2}\right)\right] \quad [20]$$

where, $$D = \frac{k'_1\, J_0(k'_1 a)}{\epsilon_{r1}\, k\, J_1(k'_1 a)}$$ [20a]

Case B : Surface and End Radiation.

The resultant field at P due to radiation from both surface and end is

$$\mathbf{E}_P = \mathbf{E}_{PS} = + \mathbf{E}_{pe}$$

which reduces to [21]

$$|E_p| = [(A')^2 + (B')^2 + 2\, A'B' \sin x]^{1/2}$$

where, $x=(L/2)\ (\beta-k\cos\theta)$

$$A'=\left(\frac{B}{2r}\left\{\frac{\mu_0}{\epsilon_0}\right\}^{1/2} k\,k'_1\ L\ a\ J_1(k'_1 a)\right)\times$$

$$\left(\frac{\sin x}{x}\left\{J_0(ka\sin\theta)\sin\theta-C\,J_1(ka\sin\theta\right\}\right) \qquad [21a]$$

$$B'=\left(\frac{B\,(\mu_0/\epsilon_0)^{1/2}\,k\,k'_1\ a\,J_1(k'_1 a)}{2\,r}\right)\times$$

$$\left(\left\{k\cos\theta+\frac{\beta}{\epsilon r_1}\right\}\left\{\frac{J_0(ka\sin\theta)\sin\theta-D\epsilon_{r_1}J_1(ka\sin\theta)}{(k'_1)^2-(k\sin\theta)^2}\right\}\right) \qquad [21b]$$

3.4 *Radiation Patterns.*

Radiation patterns (some of which are shown in Fig. 3) computed with the aid of a digital computer (Type Elliot 803) for L varying from λ_0 to $20\lambda_0$ and $a=1.27$cm. and a varying from 1.27cm. to 2.54cm. for $L=10\lambda_0$ show that

(i) For rods of smaller radii, the nature of the patterns and positions of maxima remain the same in class A and B. But in case B. the side lobe levels are higher than those in Case A.

(ii) For rods of larger radii, position of major lobe in cases A and B are different.

(iii) In all the cases, the radiation patterns have null in the forward direction ($\theta=0°$).

Figures 4 and 5 showing the variation of the position of first maxima and major lobe with respect to the length of the rod indicate (iv) a shift of the first maxima towards the axis as L is varied from λ_0 to $10\lambda_0$ The position then shifts away from the axis as L is increased from $10\ \lambda_0$ to $12\ \lambda_0$. As L is increased further from $12\ \lambda_0$ to $20\ \lambda_0$. the maxima shifts towards the axis.

(v) The position of first maxima and major lobe with respect to the radius of the rod is very sensitive to changes in radius of the rod (See Figures 6 and 7).

(vi) The variation of the number of lobes as a function of Length 'L' and radius 'a' of the rod is shown in Figures 8 and 9. Only those lobes which are above -20 *db* level are considered. The number of lobes increases with increase in length, whereas, the number of lobes first increases with increasing radius and then decreases.

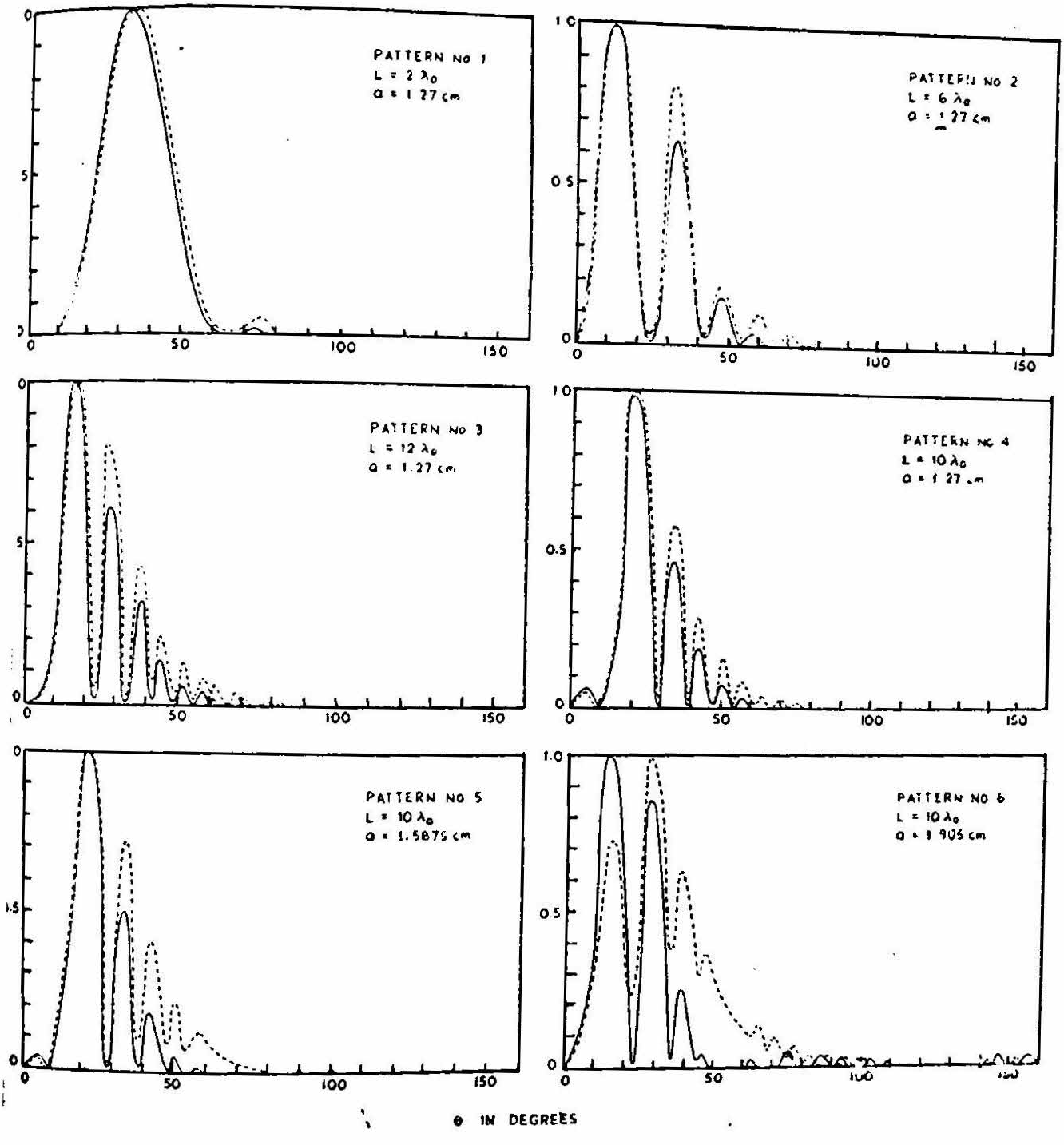

FIG. 3

Radiation patterns (power) of uniform dielectric rods. (Theoretical) E_0 mode

L = Lenth of the rod a = Radius of the rod $\lambda_0 = 3.14$ cm.

—— Case A : Considering the surface radiation only

- - - - Case B : Considering the surface and free end radiation

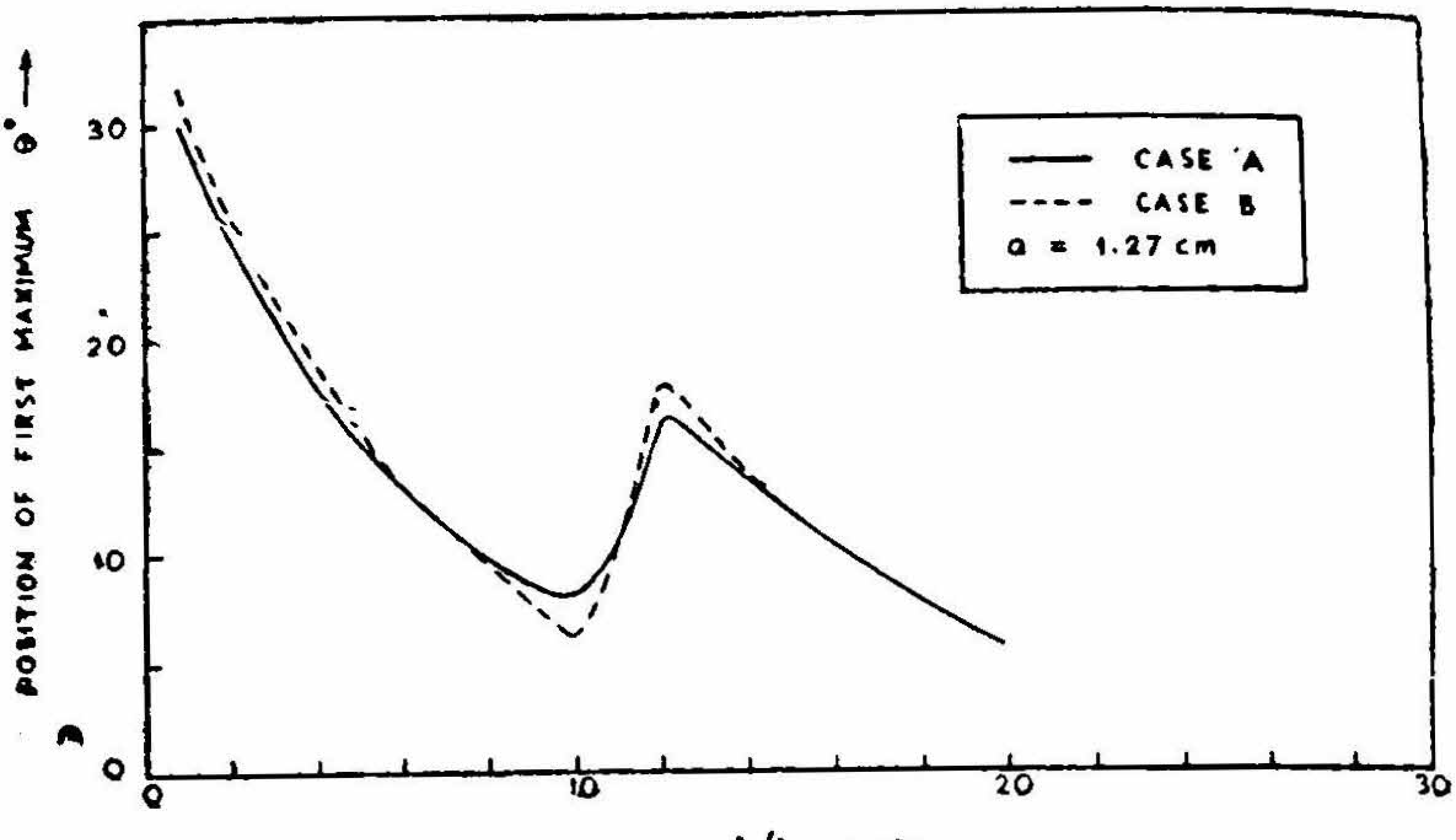

FIG. 4

Position of first maximum vs L/λ_0 for uniform dielectric rod

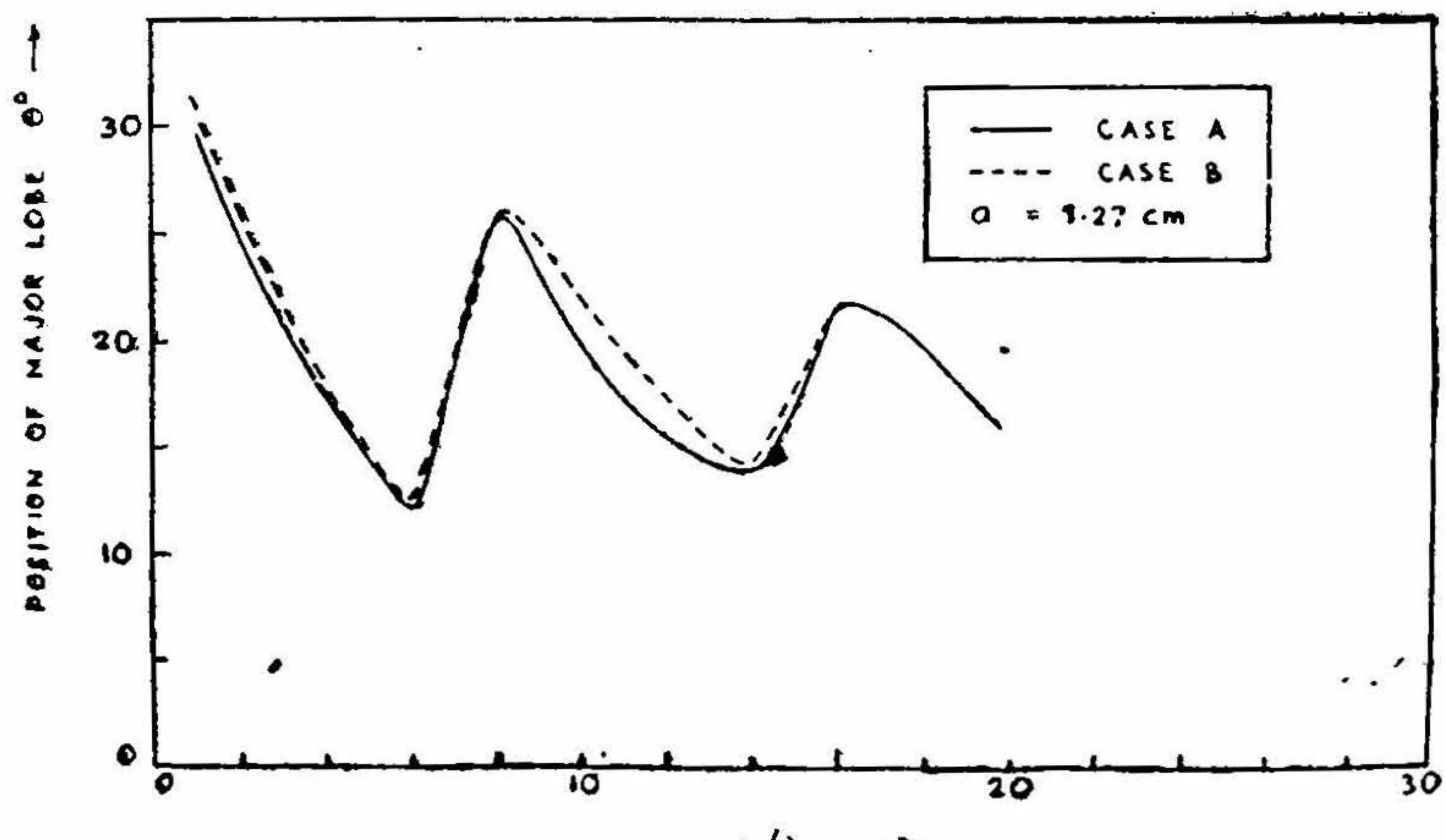

FIG. 5

Position of major lobe vs L/λ_0 for uniform dielectric rod

L = Length of the rod a = Radius of the rod λ_0 = 3.14 cm.

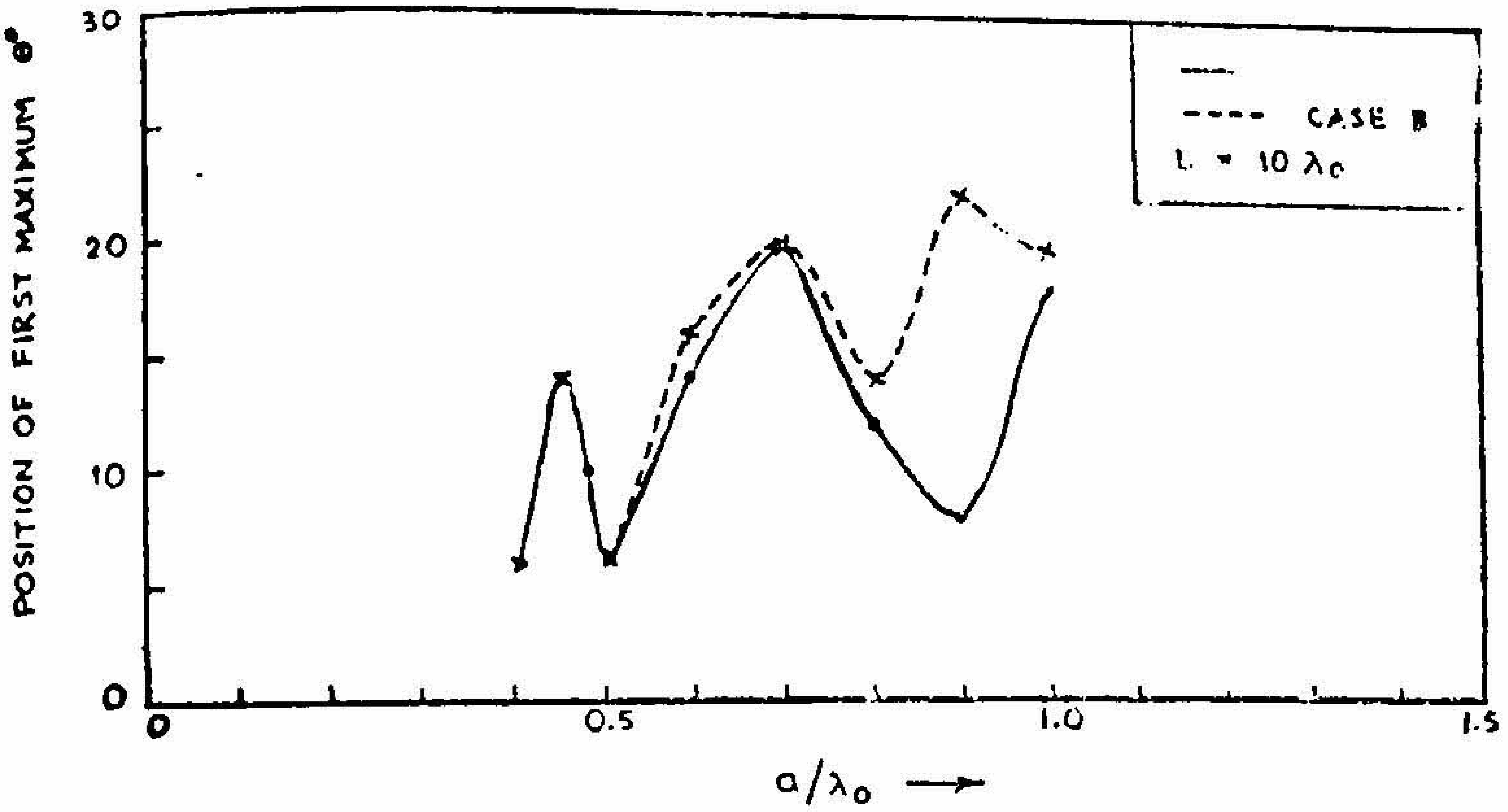

Fig. 6

Position of first maximum vs a/λ_0 for uniform dielectric rod

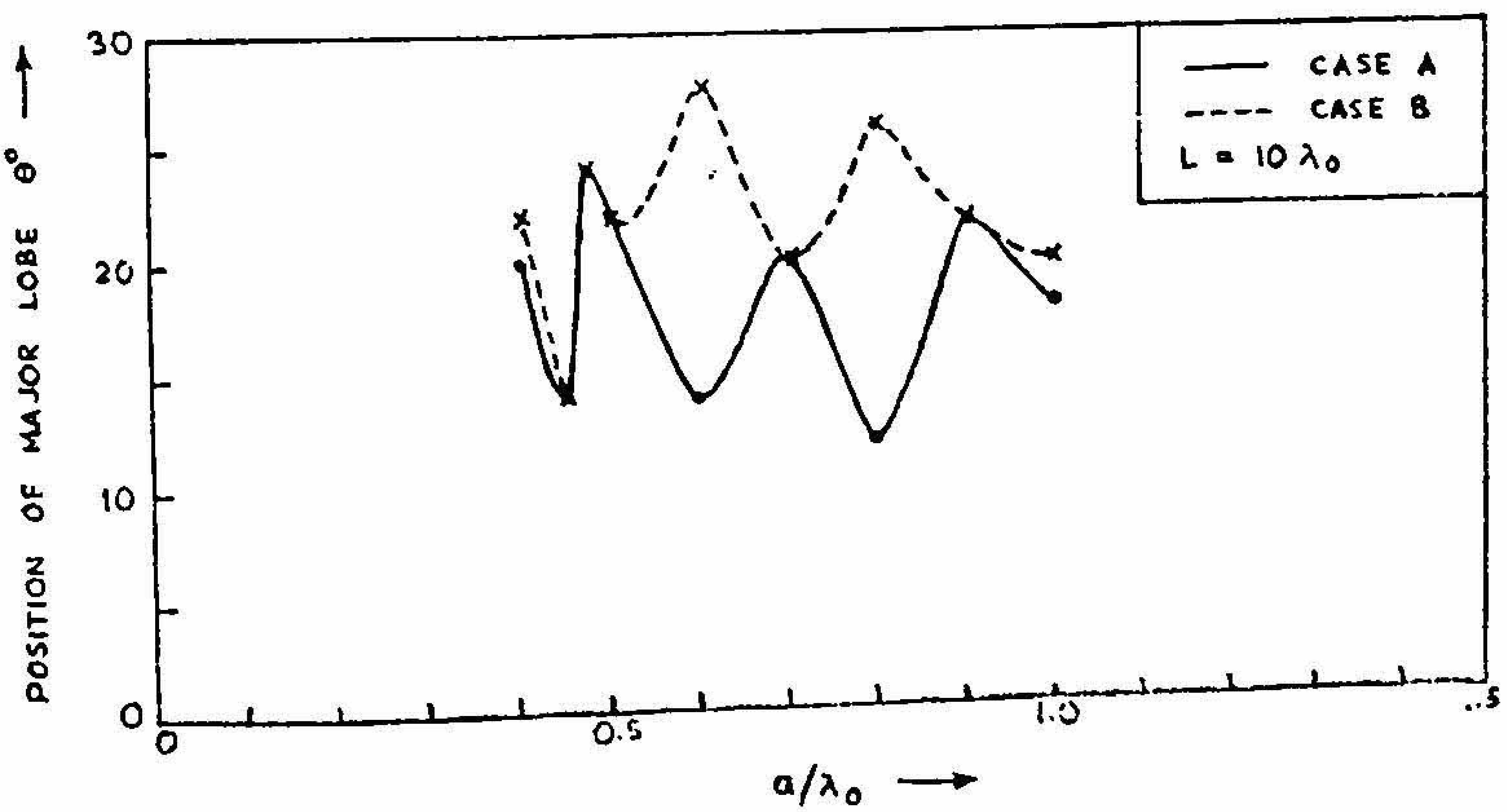

Fig. 7

Position of major lobe vs a/λ_0 for uniform dielectric rod

L-Length of the rod a-Radius of the rod λ_0=3.14 cm.

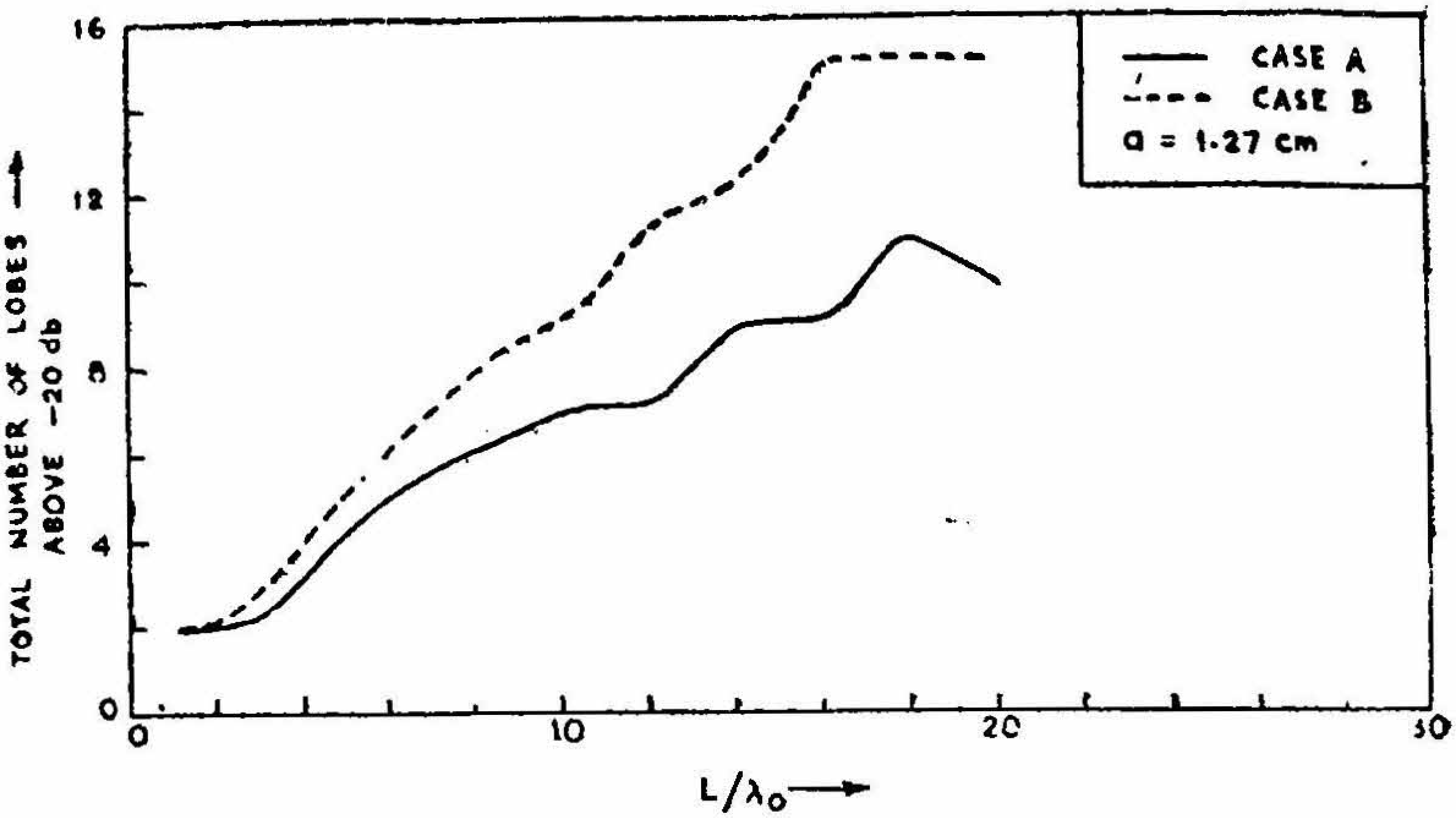

FIG. 8

Number of lobes vs L/λ_0 for uniform dielectric rod

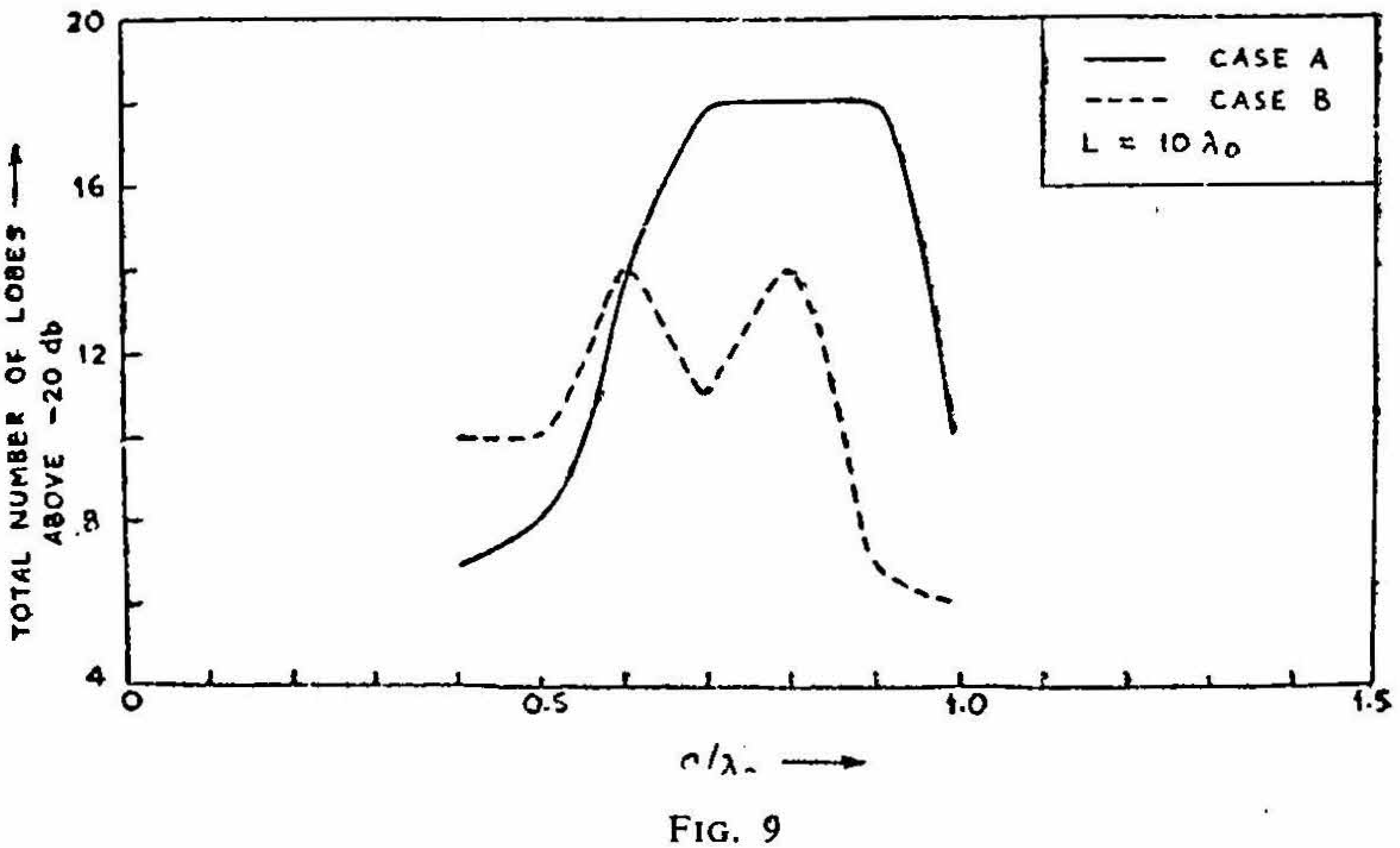

FIG. 9

Number of lobes vs a/λ_0 for uniform dielectric rod

L = Length of the rod a = radius of the rod λ_0 = 3.14 cm.

(vii) The $3-db$ beam width of the major lobe decreases with increasing length of the rod (See Fig. 10), whereas, the $3-db$ beam width of the major lobe remains almost the same within ± 2 with increasing radius of the rod (See Fig. 11).

A complete analysis of the radiation patterns of uniform dielectric rod is given in Table 2 and 3.

4. Radiation from Corrugated Dielectric Rod

In this case also the radiation pattern calculations have been made for case *A* and case *B*.

4.1 *Field Components*

The field components in the three different regions (See Fig. 12) of the corrugated dielectric rod are

Region 1 : a

$$E_{z1} = A_1 \, J_0(k_1\rho) \exp(-j\beta z)$$

$$E_{\rho 1} = A_1 \, (j\beta/k_1) \, J_1(k_1\rho) \exp(-j\beta z)$$

$$H_{\phi' 1} = A_1 (j\omega\epsilon_1/k_1) \, J_1(k_1\rho) \exp(-j\beta z) \qquad [22]$$

Region 2 : $a \leqslant \rho \leqslant b$

$$E_{z2} = A_2 \, J_0(k_2\rho) + A_3 Y_0(k_2\rho) \exp(-j\beta z)$$

$$E_2 = (j\beta/k_2) \, [A_2 \, J_1(k_2\rho) + A_3 Y_1(k_2\rho)] \exp(-j\beta z)$$

$$H_{\phi' 2} = (j\omega\epsilon_2/k_2) \, [A_2 \, J_1(k_2\rho) + A_3 Y_1(k_2\rho) \exp(-j\beta z)] \qquad [23]$$

Region 3 : $\rho \geqslant b$

$$E_{z3} = A_4 H_0^{(1)}(k_3\rho) \exp(-j\beta z)$$

$$E_3 = (j\beta/k_3) \, H_1^{(1)}(k_3\rho) \exp(-j\beta z)$$

$$H_{\phi' 3} = A_4 \, (j\omega\epsilon_0/k_3) \, H_1^{(1)}(k_3\rho) \exp(-j\beta z) \qquad [24]$$

where, $$\epsilon_2 = \epsilon_0 \, \epsilon_{r2} = \epsilon_0 \left(\frac{\sqrt{(\epsilon_{r1})} \, t + s}{t+s} \right)^2 \qquad [25]$$

is the effective permittivity of the corrugated medium derived by equating the optical path lengths and assuming plane wave propagation in the second medium. (See Fig. 12)

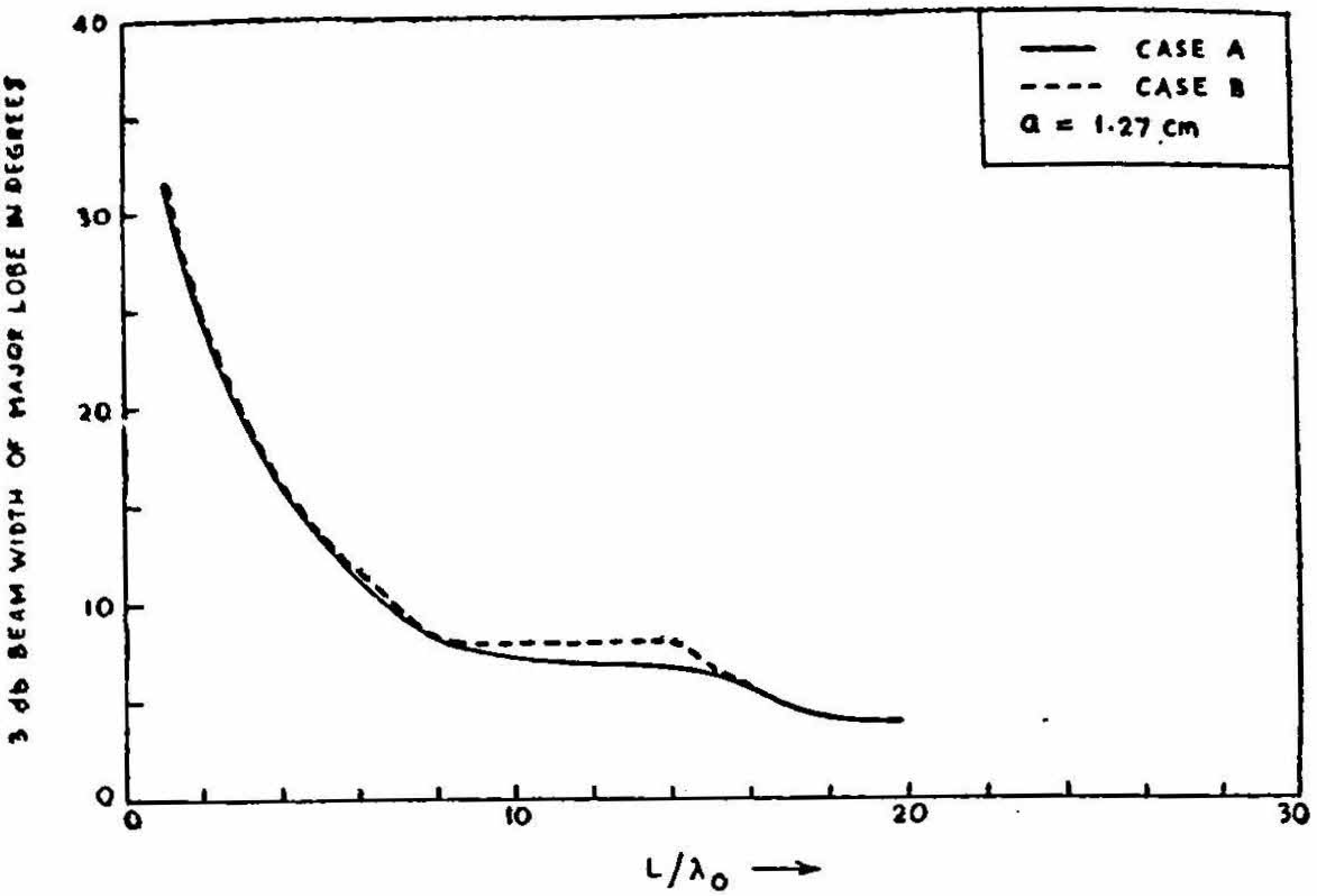

FIG. 10

$3\,db$ beam width of major lobe vs L/λ_0 for uniform dielectric rod

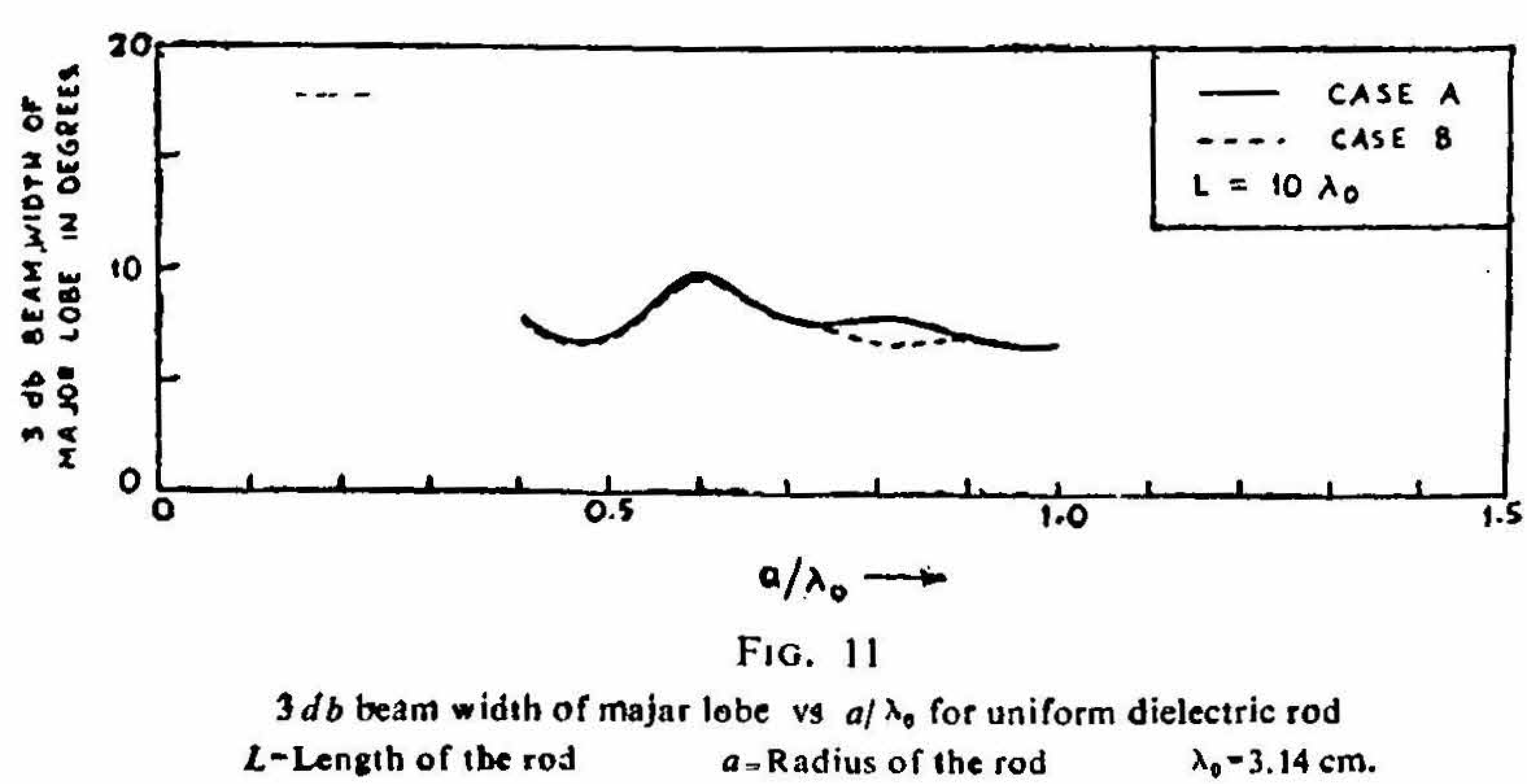

FIG. 11

$3\,db$ beam width of majar lobe vs a/λ_0 for uniform dielectric rod

L-Length of the rod a=Radius of the rod λ_0=3.14 cm.

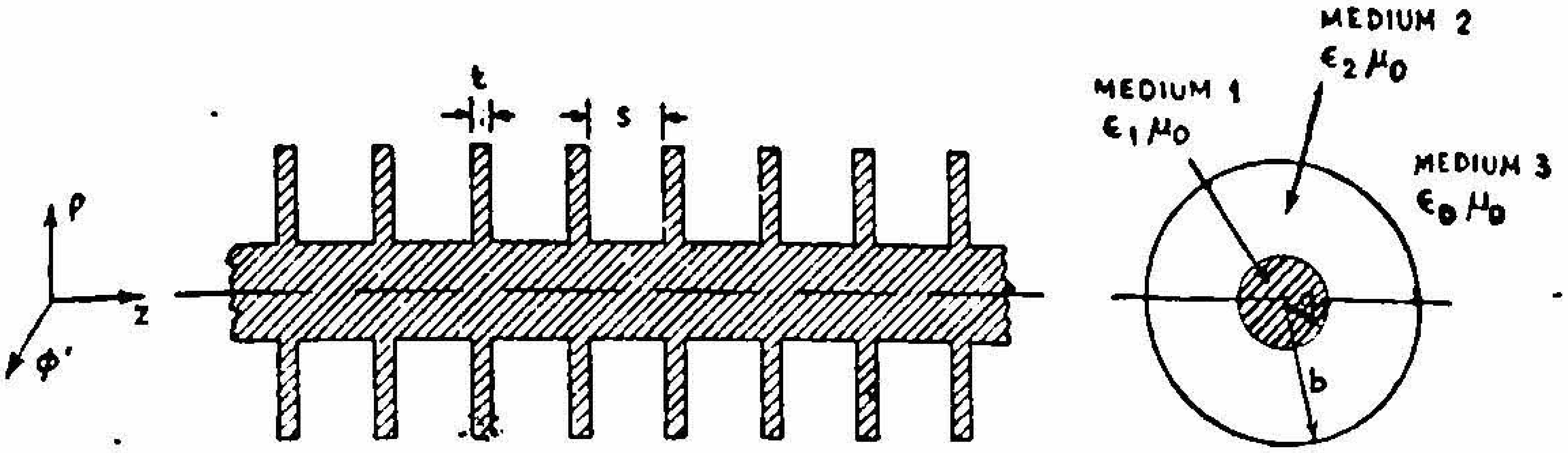

FIG. 12

Corrugated dielectric rod

a = Radius of the inner rod
b = Radius of disc
t = Thickness of disc
s = Spacing between discs

ϵ_1 = Permittivity of medium 1
ϵ_2 = Permittivity of medium 2
ϵ_0 = Permittivity of free space (mediun 3)
μ_0 = Permeability of free space

Medium 1 : $\rho \leq a$
Medium 2 : $a \leq \rho \leq b$
Medium 3 : $\rho \geq b$

4.2 *Evaluation of the Radiation Field of a corrugated Dielcctric Rod*

Case A : The electric and magnetic current sheets

On the surface coincident with the circumference ($\rho = b$) of the dielectric discs and extending all along the length of the rod are

$$\mathbf{J} = \mathrm{z} H_{\phi'} = \mathrm{Z}\ C_3' \exp\left(-j\beta z\right) \qquad [26]$$

where, $C_3' = (j\omega\epsilon_2/k_2)\ [A_2\ J_1(k_2 b) + A_3 Y_1(k_2 b)]$ [26a]

$$\mathbf{M} = \vec{\phi}'\ C_2' \exp\left(-j\beta z\right) \qquad [27]$$

where, $C_2' = A_2\ J_0(k_2 b) + A_3 Y_0(k_2 b)$ [27a]

The far field due to the surface radiation from the corrugated rod is obtained similarly as in previous section.

$$\mathbf{E}_{PS} = [(-\,j\,b/4\,\pi r)\exp j\,(\omega\,t - kr)\int_0^L \exp -j\,(\beta z + kz)\cos\theta\; dz] \times$$

$$[\{\vec{\theta}\int_0^{2\pi}\omega\mu_0\,(-\sin\theta)\; C_3' \exp\left[j\,u\cos\left(\phi' - \phi\right)\right] d\,\phi'\}$$

$$+\{\vec{\theta}\int_0^{2\pi} k\; C_2' \cos\left(\phi' - \phi\right) \exp j\,u\cos\left(\phi' - \phi\right)\, d\,\phi'\}$$

$$+\{\vec{\phi}\int_0^{2\pi} k\; C_2' \cos\theta\,\sin\left(\phi' - \phi\right) \exp j\,u\cos\left(\phi' - \phi\right)\, d\,\phi'\}]$$

which reduces to

$$\mathbf{E}_{PS} = \left(\left\{ -\frac{1}{2r} \frac{b\,L\,k^2\,\epsilon_{r2}}{k_2} \right\} \{A_2\,J_1(k_2b) + A_3Y_1(k_2b)\} \{\exp -(\,j\;L/2)(\beta - k\cos\theta)\} \times \{ J_0(kb\sin\theta)\sin\theta - C''\,J_1(kb\sin\theta)\} \frac{\sin x}{x} \right) \quad [28]$$

where,

$$u = k\,a\sin\theta \text{ and } x = (L/2)\,(\beta - k\cos\theta)$$

$$C'' = \frac{k_2}{k\epsilon_{r2}} \left(\frac{A_2\,J_0(k_2b) + A_3Y_0(k_2b)}{A_2\,J_1(k_2b) + A_3Y_1(k_2b)} \right) \quad [28a]$$

Case A' : Free End Radiation

The free end is assumed to be terminated by a disc of radius 'a'. The electric and magnetic current sheets are

$$\mathbf{J} = \mathbf{z} \times \vec{\phi}'\;H_{\phi'} = -\vec{\rho} H_{\phi'} = \vec{\rho}\;D'_1\;J_1(k_1\rho) \quad [29]$$

$$\mathbf{M} = -\mathbf{z} \times \vec{\rho}\;E_\rho = -\vec{\phi}'\;E_\rho = \phi'\;D'_2\;J_1(k_1\rho) \quad [29a]$$

wheee, $D'_1 = -(\,j\omega\epsilon_1/k_1)\;A_1$ [30]

and $D'_2 = -(\,j\beta A_1/k_1)$ [30a]

The field at P due to radiation from the end of the rod is

$$E_{P_e} = \left[(\,jA_2) \left\{ \frac{A_1}{A_2} \left(\frac{k^2\epsilon_{r1}\cos\theta}{k_1} + \frac{k\beta}{k_1} \right) a \right\} \right] \left(\frac{k_1\,J_1(ka\sin\theta)\,J_0(k_1a) - (k\sin\theta)\,J_1(k_1a)\,J_0(ka\sin\theta)}{k_1^2 - (k\sin\theta)^2} \right) \quad [31]$$

Case B : Surface and Free End Radiation

The rusultant field at P due to radiation from the surface as well as end is

$$\mathbf{E}_P = \mathbf{E}_{PS} + \mathbf{E}_{Pe}$$

which yields

$$|E_P| = [(A'')^2 + (B'')^2 + w\,A''\,B''\,\sin x]^{1/2} \quad [32]$$

where,

$$x = (L/2)\,(\beta - k\cos\theta)$$

$$A'' = \left\{\frac{A_2}{2r}\left(\frac{b\,L\,k^2\epsilon_{r2}}{k_2}\right)\left\{ J_1(k_2b) + (A_3/A_2)\,Y_1(k_2b)\right\}\right\}\left(J_0(kb \sin\theta)\sin\theta\right.$$

$$\left. -\frac{k_2}{k\epsilon_{r2}}\left[\frac{J_0(k_2b) + (A_3/A_2)\,Y_0(k_2b)}{J_1(k_2b) + (A_3/A_2)\,Y_1(k_2b)}\right] J_1(kb\sin\theta)\left(\frac{\sin x}{x}\right)\right) \qquad [32a]$$

$$B'' = \left\{ A_2\left(\frac{A_1}{A_2}\right)\frac{ka}{k_1}(k\epsilon_{r1}\cos\theta + \beta)\times\right.$$

$$\left.\times\left(\frac{k_1 J_1(ka\sin\theta)\,J_0(k_1a) - (k\sin\theta)\,J_1(k_1a)\,J_0(ka\sin\theta)}{k_1^2 - (k\sin\theta)^2}\right)\right\} \qquad [32b]$$

$$\frac{A_3}{A_2} = \frac{(k_3/k_2)\epsilon_{r2}\,[H_0^{(1)}(k_3b)/\{H_1^{(1)}(k_3b)\}]\,J_1(k_2b) - J_0(k_2b)}{Y_0(k_2b) - (k_3\epsilon_{r2}/k_2)\,[H_0^{(1)}(k_3b)/\{H_1^{(1)}(k_3b)\}]\,Y_1(k_2b)} \qquad [32c]$$

and

$$\frac{A_1}{A_2} = \frac{J_0(k_2a) + (k_3\epsilon_{r2}/k_2)\,[H_0^{(1)}(k_3b)/\{H_1^{(1)}(k_3b)\}]\,Y_0(k_2a)}{J_0(k_1a)} \qquad [32d]$$

Numerical Computations of Radiation Patterns

The radiation power patterns have been computed in both the cases *A* and *B* as functions of *t*, *s*, *a* and *b*. Some of the computed power patterns normalised with respect to the maximum value of the radiated power are shown in figures 13 and 14. The following observations based on the results of numerical computations may be of interest

(i) The radiation patterns of the corrugated dielectric rods have, in general, similar characteristics as that of the uniform dielectric rods.

(ii) The positions of the maxima appear to be almost the same in the two cases *A* and *B*

(iii) The intensity of the minor lobes appear to differ in the two cases *A* and *B*

(iv) Effect of variation of '*s*' :

The variation of the position of first maxima and the major lobe with respect to s/λ_0 for the following two structures

$t = 0.15875$ c.m.	$a = 0.9525$ cm.	$b = 1.905$ cm.
$t = 0.15875$ cm.	$a = 0.9525$ cm.	$b = 1.5875$ cm.

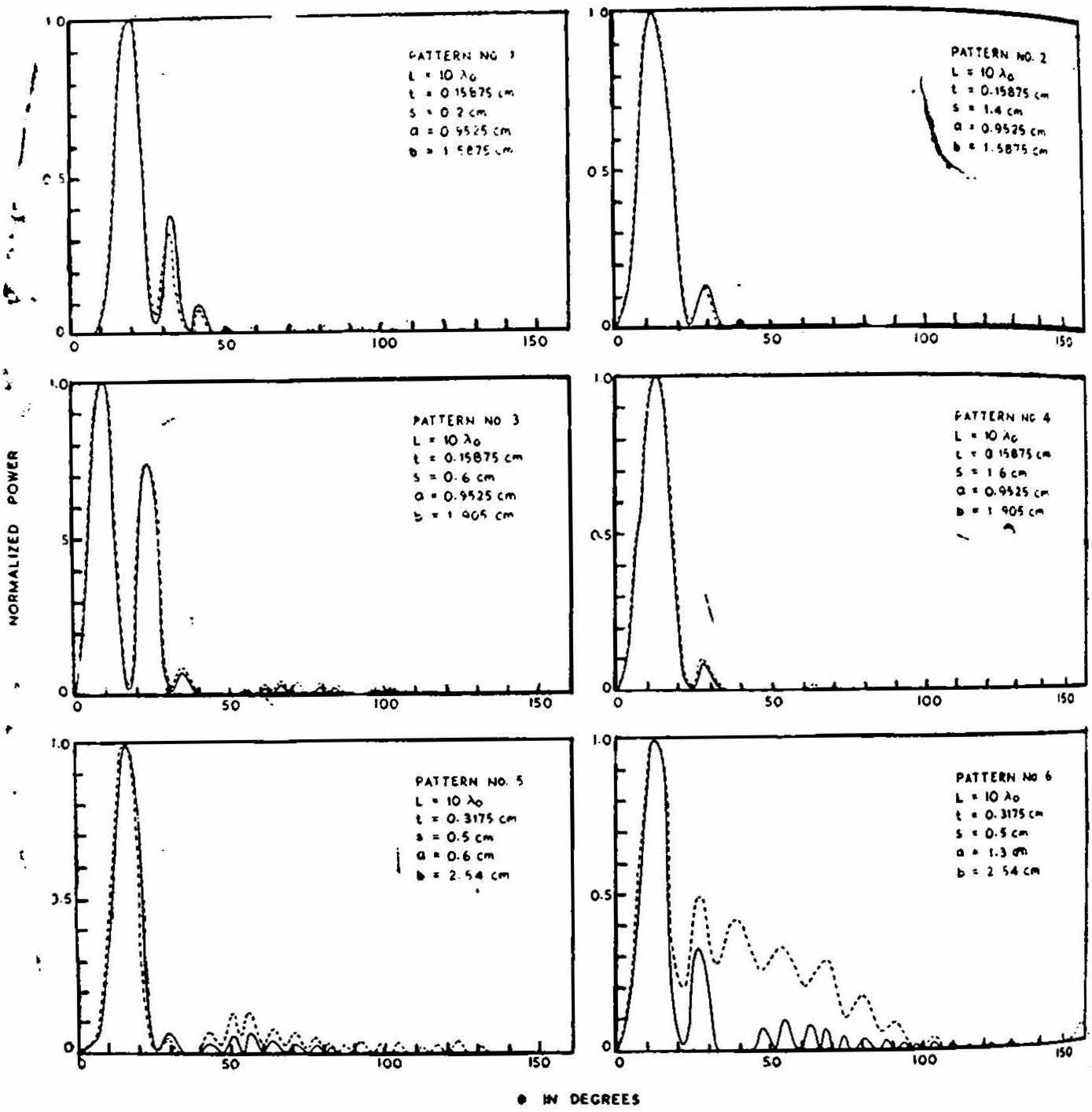

FIG. 13

Radiation patterns (power) of corrugated dielectric rods. (Theoretical) E_0 mode

L = Length of the rod t = Disc thickness s = Disc spacing
a = Inner rod radius b = Disc radius $\lambda_0 = 3.14$ cm.

—— Case A : Considering the surface radiation only
- - - - Case B : Considering the surface and free end radiation

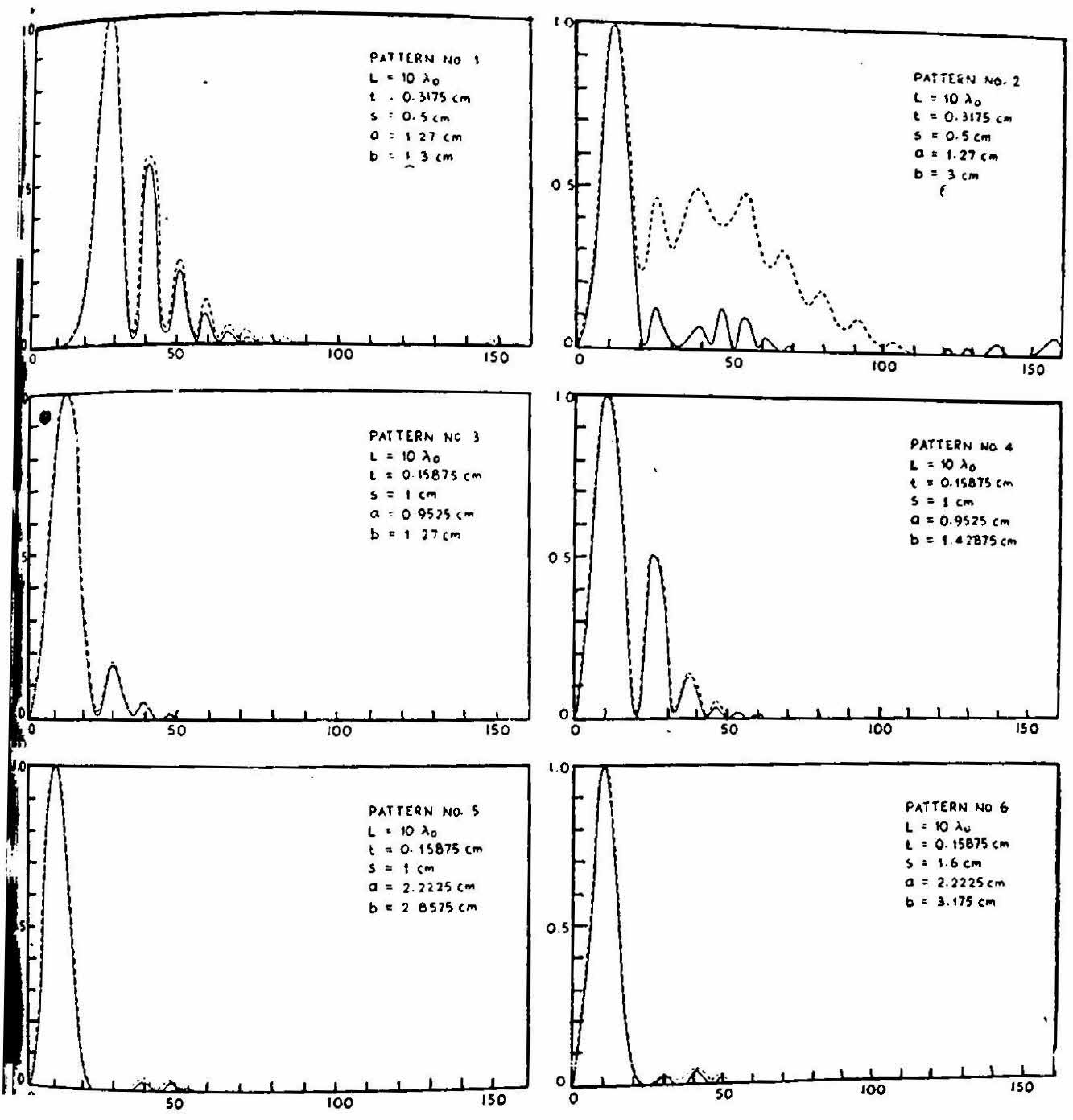

FIG. 14

Radiation patterns (power) of corrugated dielectric rods. (Theoretical) E_0 mode

L = Length of the rod t = Disc thickness s = Disc spacing
a = Inner rod radius b = Disc radius λ_0 = 3.14 cm.

—— Case *A*: Considering the surface radiation only
- - - - Case *B*: Considering the surface and free end radiation.

and 's' varying from 0.1 cm. to 1.6 cm. shows (See Figures 15 and16) that

(*a*) the position of the first maxima and the position of the major lobe oscillates in the beginning and then become constant for large values of s/λ_0. The nature of variation in the two cases A and B is almost the same.

(*b*) The number of lobes decreases with increasing s/λ_0 in the beginning and then becomes fairly constant. There is a marked difference in the number of lobes between the two cases A and B (See Figures 17 and 18).

(*c*) The $3-db$ beam width of the major lobe oscillates as a function of s/λ_0 around a mean value of about $\pm 2°$ to $\pm 3°$ (See Figures 19 and 20).

(v) Effect of variation of 'a'.

Figures (21–24) show the different characteristics as fuuctions of a/λ_0 for the following combinations of structure parameters

$t=0.3175$ cm, $s=0.5$ cm. $b=2.54$ cm.

$t=0.15876$ cm. $s=1$ cm. $b=1.5875$ cm.

The characteristics are very sensitive to the variation of 'a'.

(vi) Effect of variation of 'b'

Figures (25-28) show the variation of characteristics as a function of b/λ_0 for the following combinations of structure parameters

$t=0.3175$ cm, $s=0.5$ cm, $a=1.27$ cm.

$t=0.15875$ cm, $s=0.5$ cm, $a=1.27$ cm.

The characteristics are sensitive to the changes of b/λ_0 when its values are smaller but the characteristics show fairly constant behaviour for larger values of b/λ_0.

5. GAIN

The radiation pattern consists of an off-axis major lobe and a number of secondary lobes. The gain is referred to the direction of maximum radiation.

5.1 *Gain of Uniform Dielectric Rod*

If the radiation from the junction of the launcher and the rod is ignored, the total power flow P_{zt} which consists power flow P_z^i inside the rod and power flow P_z^0 outside the rod is given by

$$P_{zt}=P_z^i+P_z^0 \qquad [33]$$

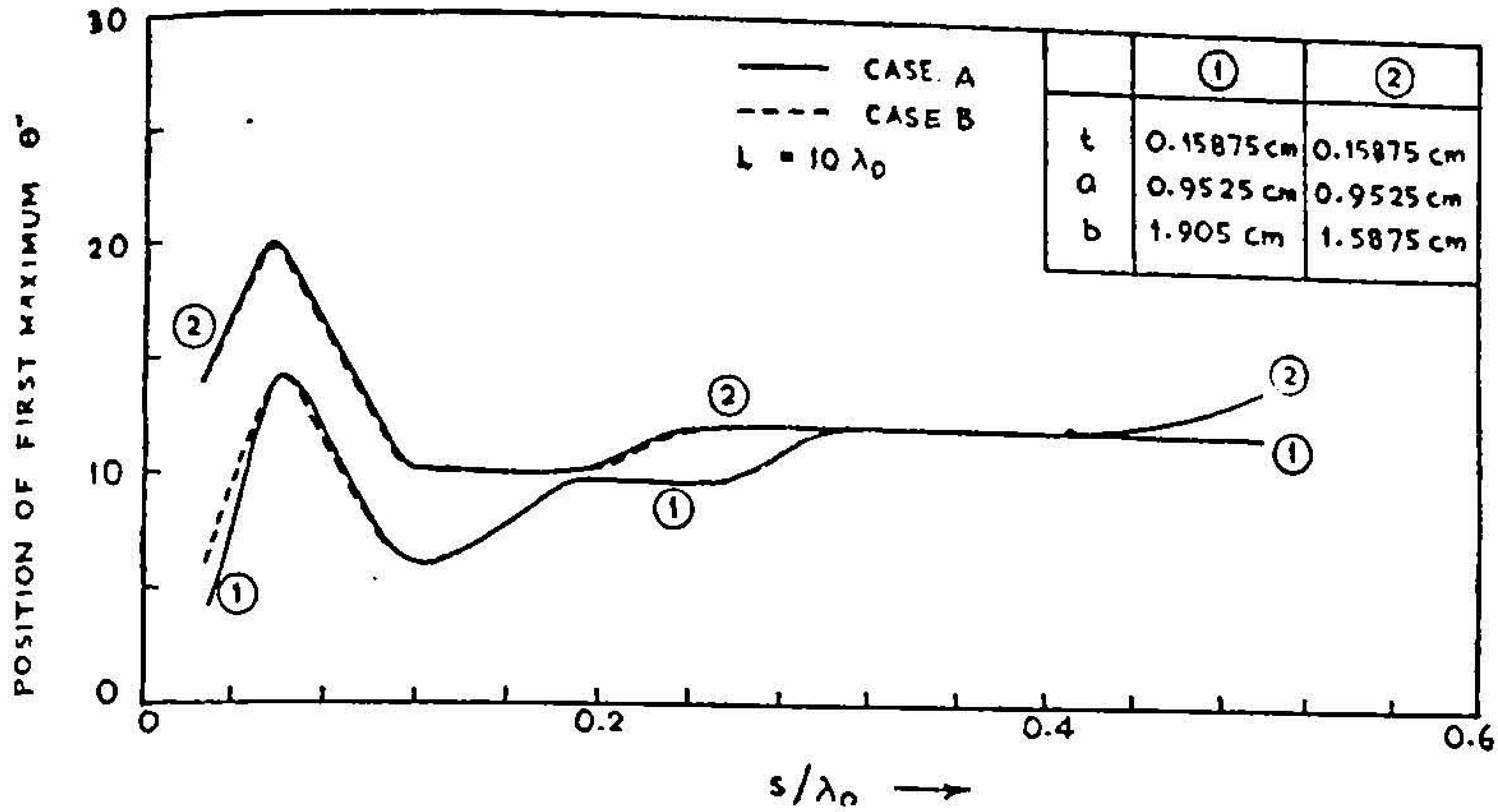

FIG. 15

Position of first maximum vs s/λ_0 for coorrugated dielectric rod

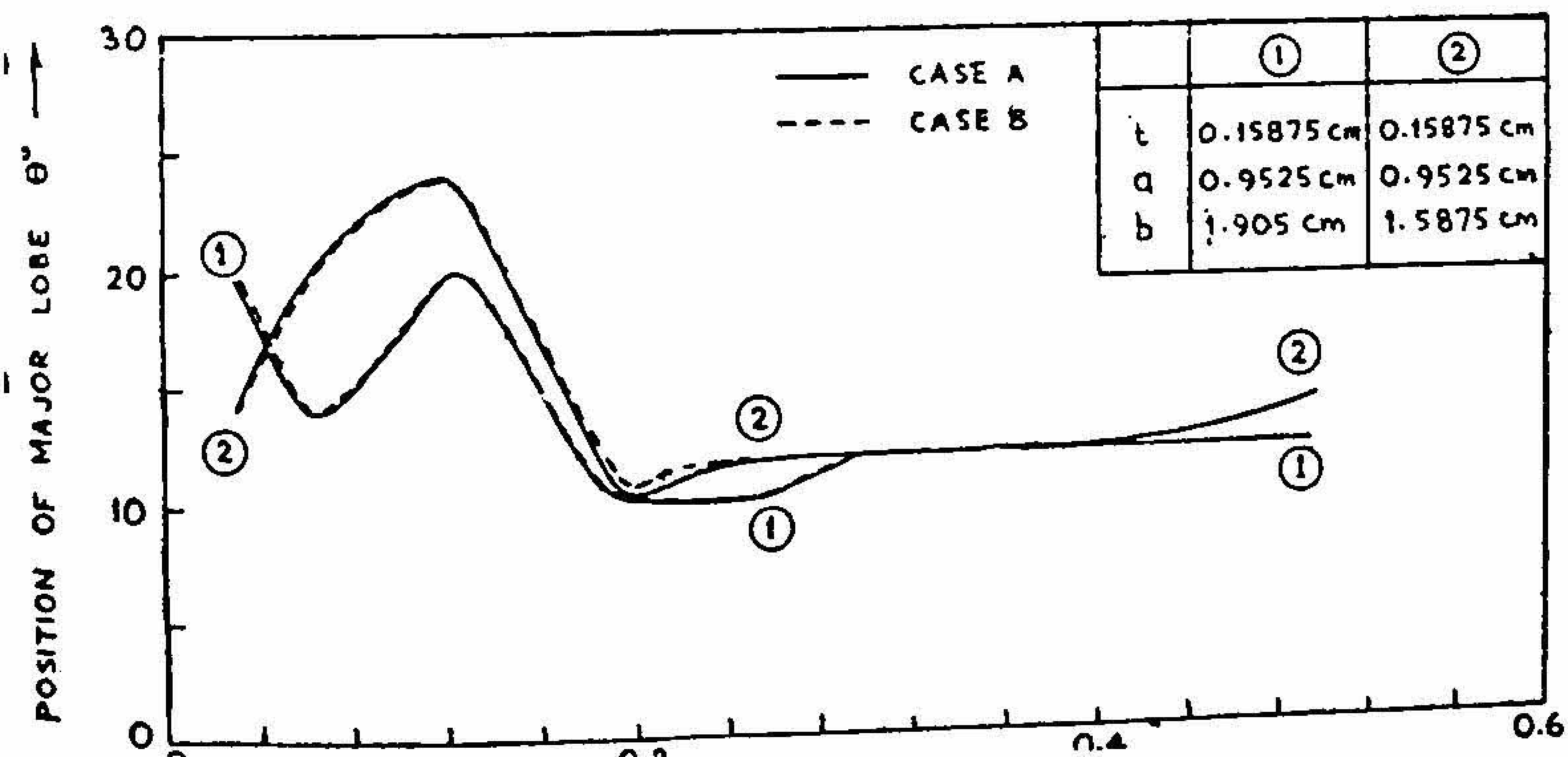

FIG. 16

Position of major lobe vs s/λ_0 for corrugated dielectrie rod

L = Length of the rod
t = Disc thickness
s = Disc spacing
a = Inner rod radius
b = Disc radius
λ_0 = 3.14 cm.

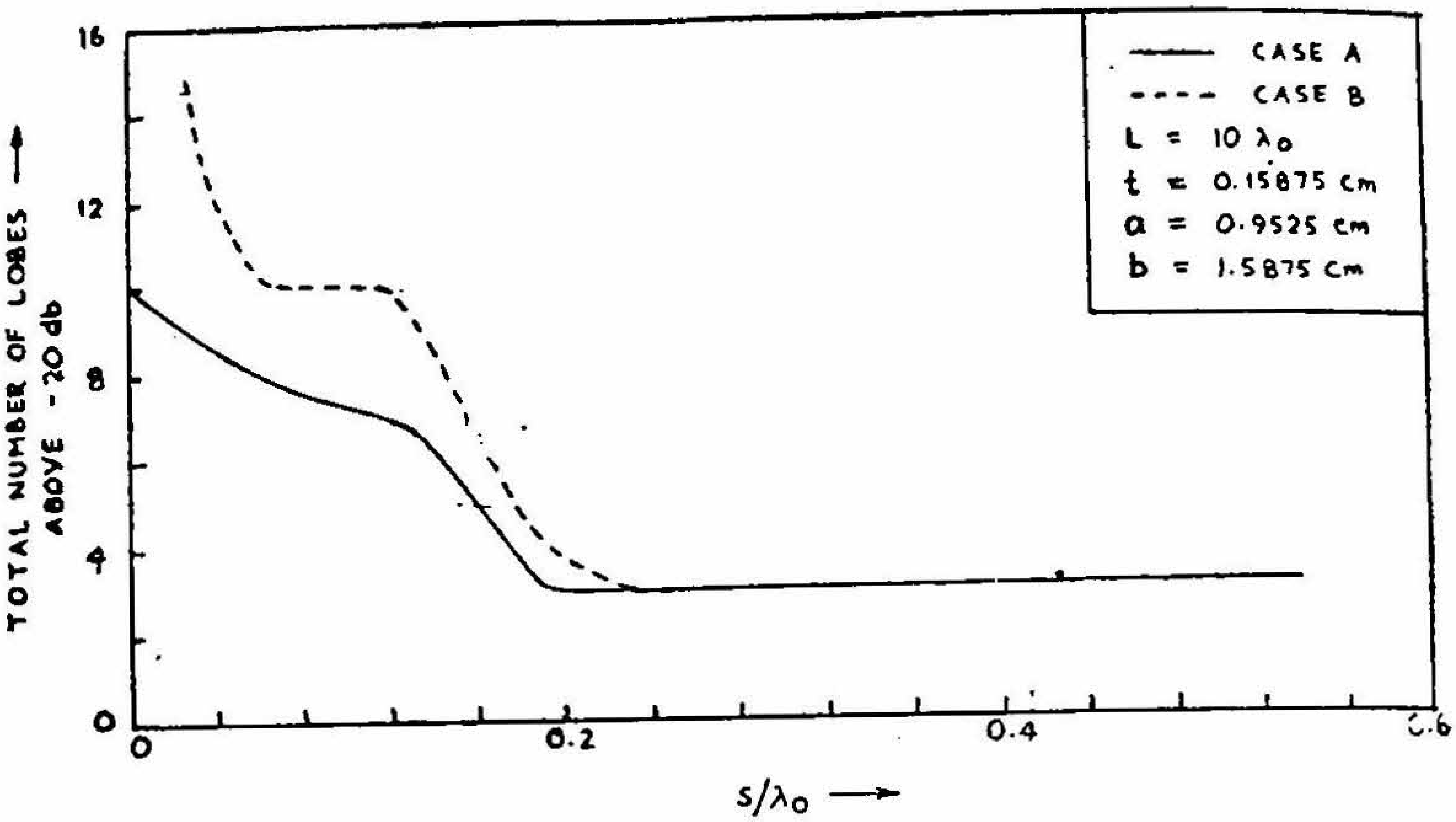

FIG. 17

Number of lobes vs s/λ_0 for corrugated dielectric rod

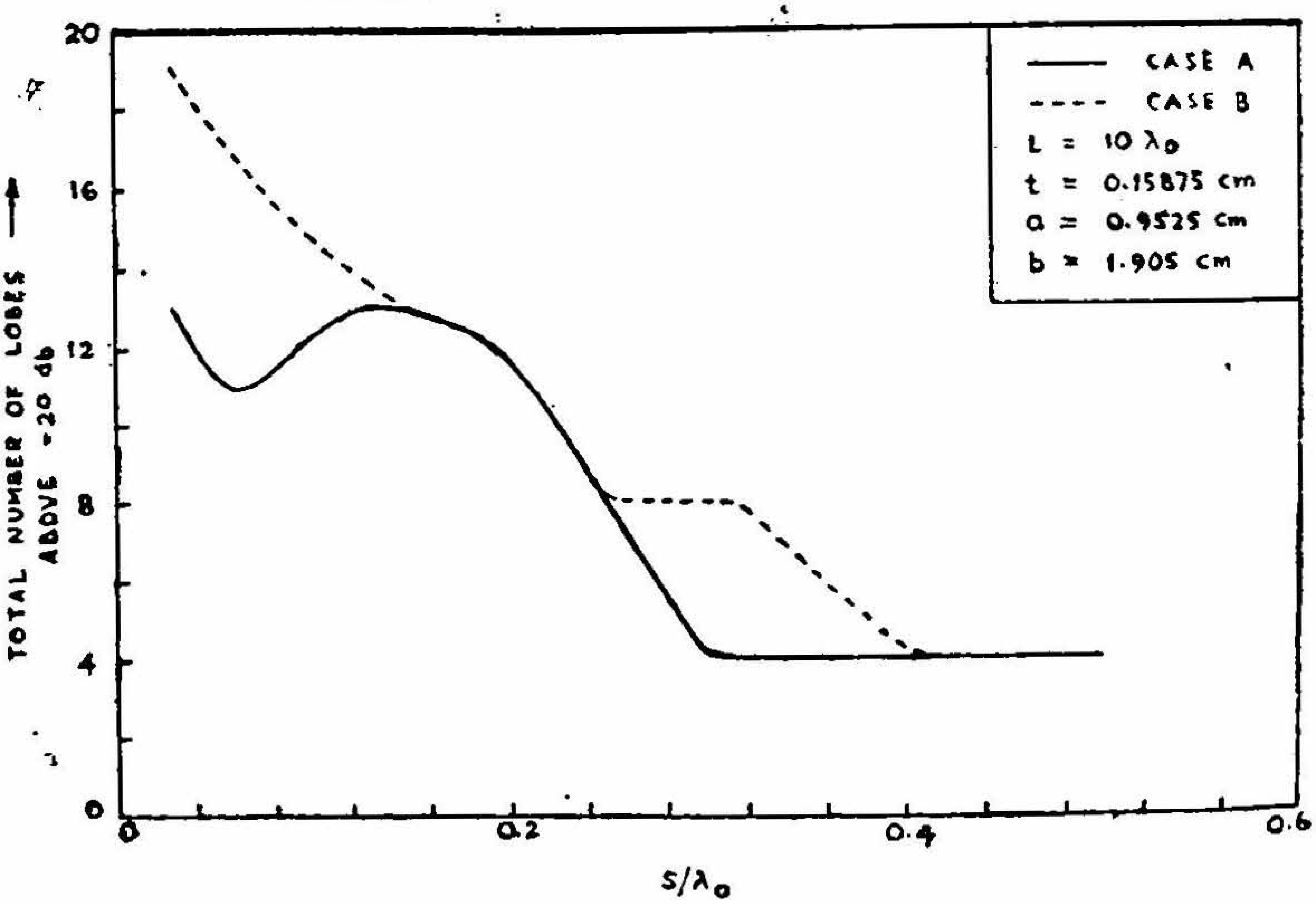

FIG. 18

Number of lobes vs s/λ_0 for corrugated dielectric rod

L = Length of the rod s = Disc spacing b = Disc radius
t = Disc thickness a = Inner rod radius λ_0 -3.14 cm

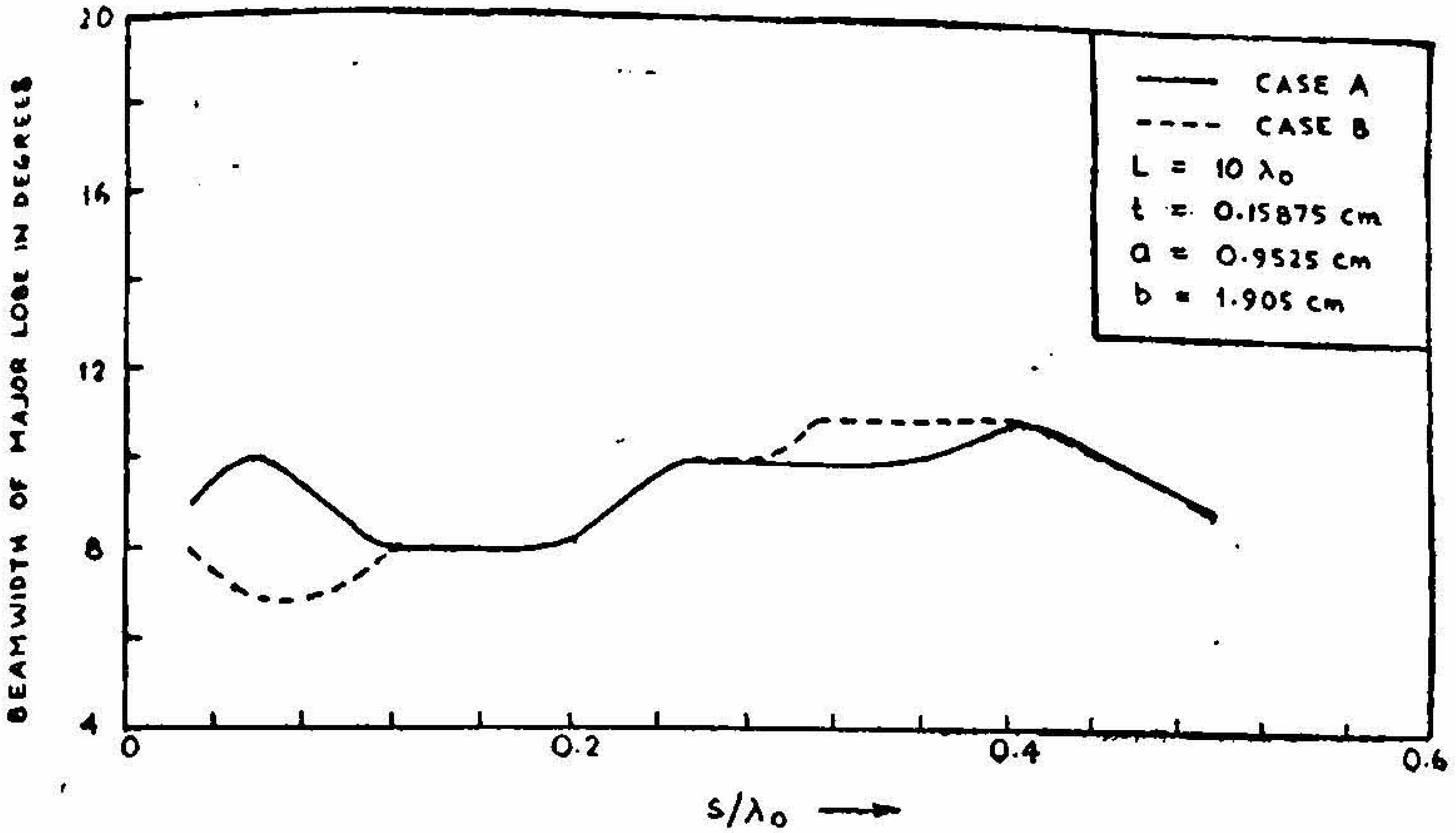

FIG. 19

Beam width of the major lobe vs s/λ_0 for corrugated dielectric rod

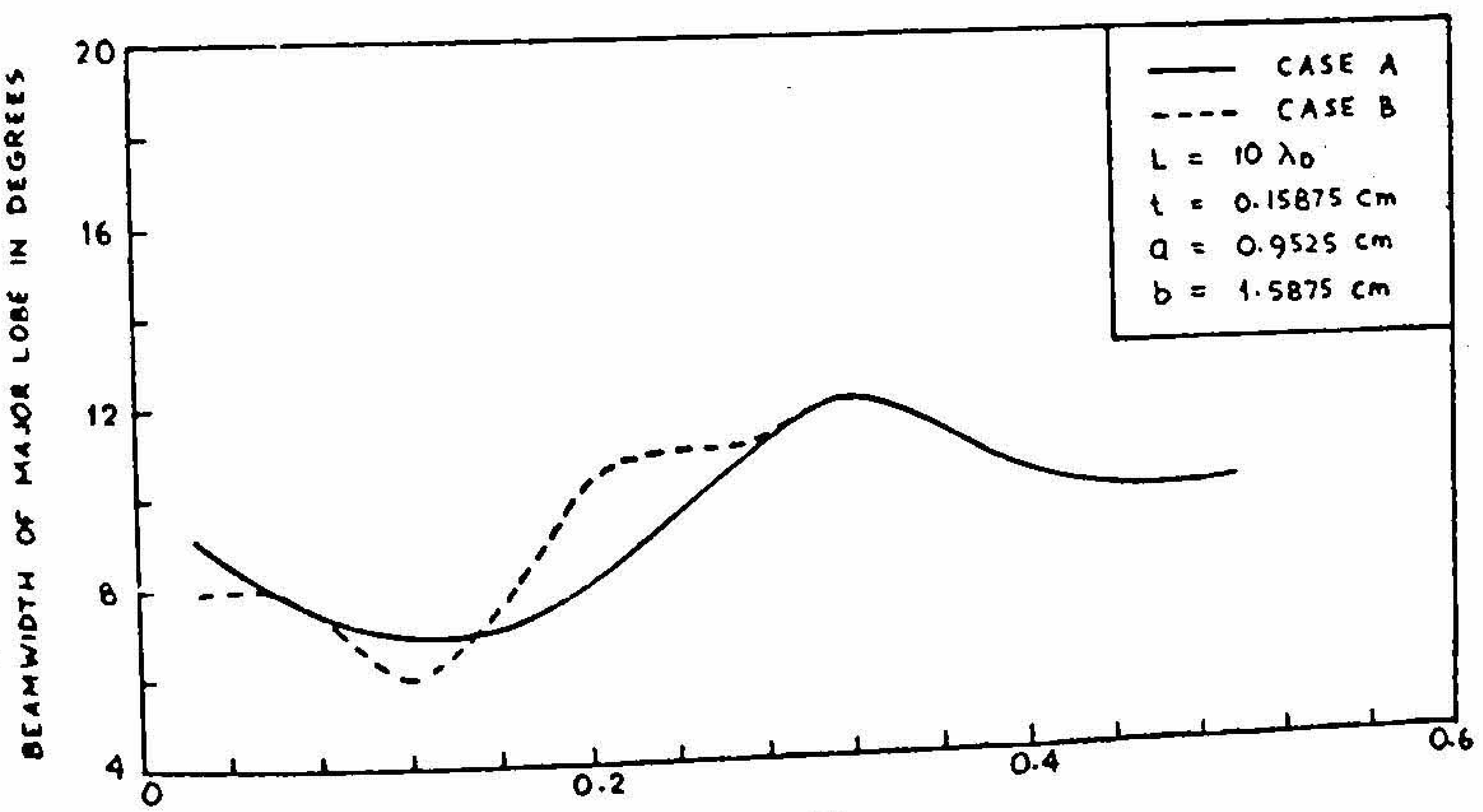

FIG. 20

Beam width of the major lobe vs s/λ_0 for corrugated dielectric rod

L=Length of the rod s=Disc spacing b=Disc radius
t=Disc thickness a=Inner rod radius λ_0=3.14 cm.

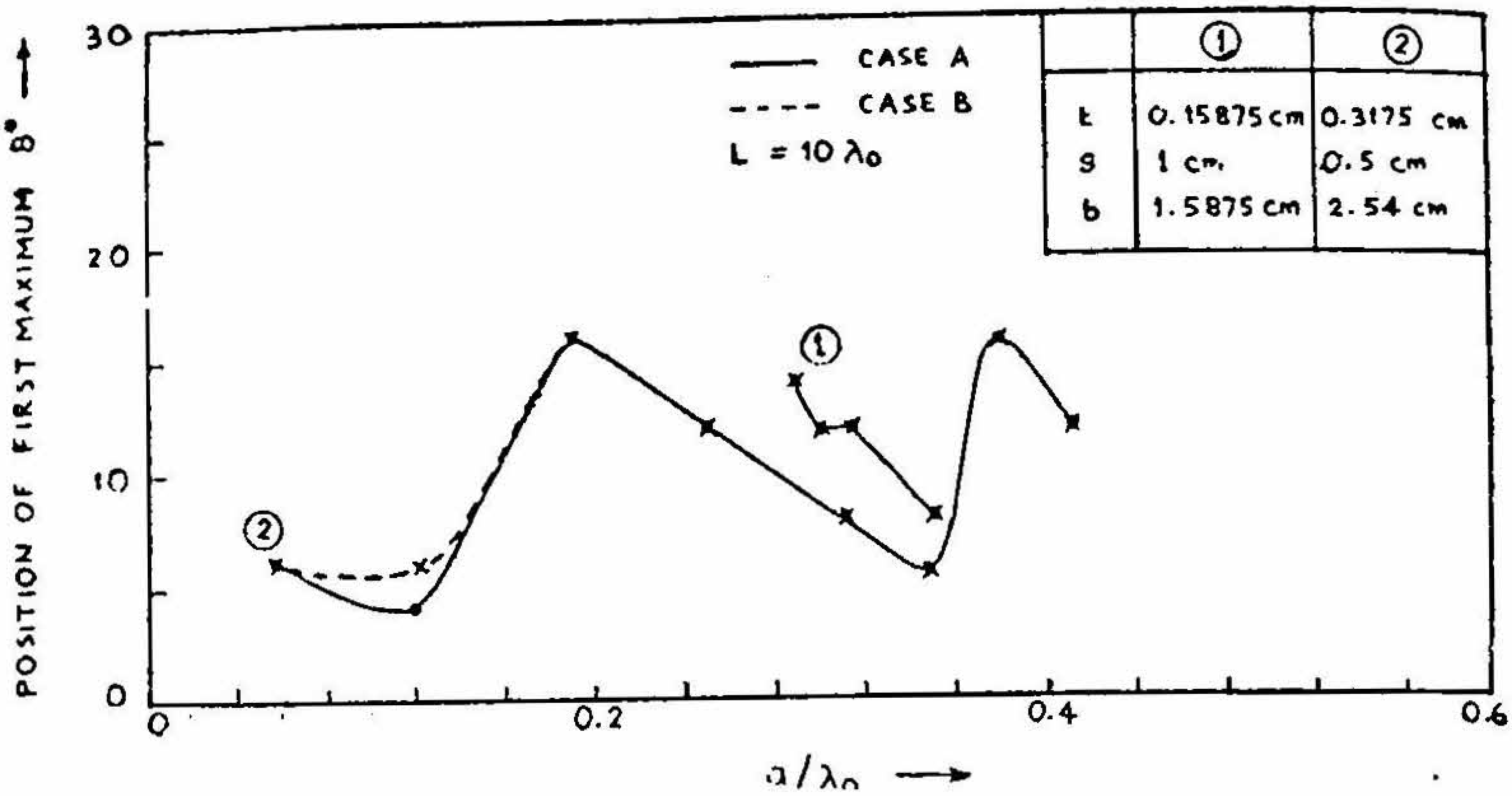

FIG. 21

Position of first maximum vs a/λ_0 for corrugated dielectric rod

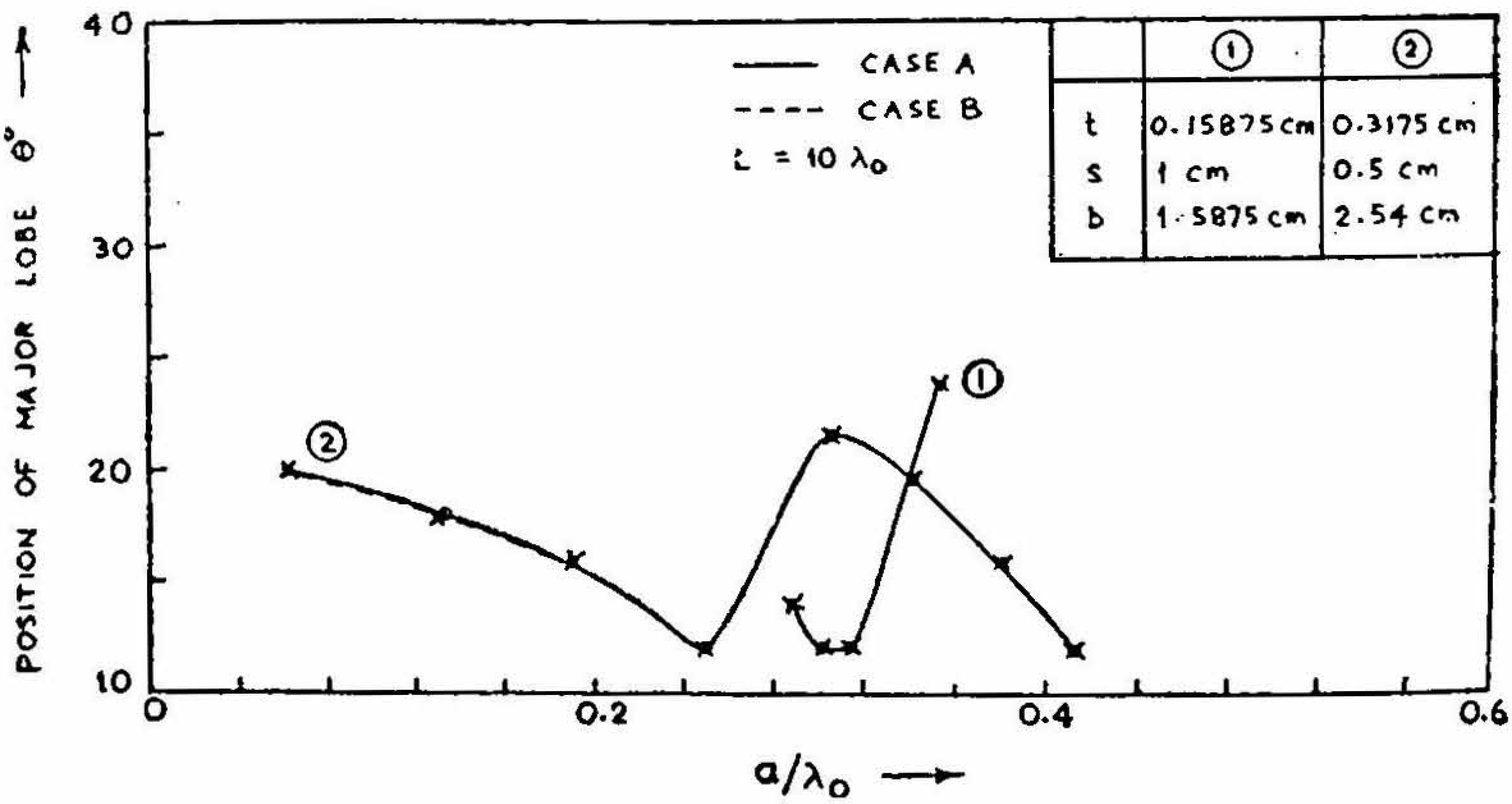

FIG. 22

Position of major lobe vs a/λ_0 for corrugated dielectric rod

L = Length of the rod s = Disc spacing b = Disc radius
t = Disc thickness a = Inner rod radius $\lambda_0 = 3.14$

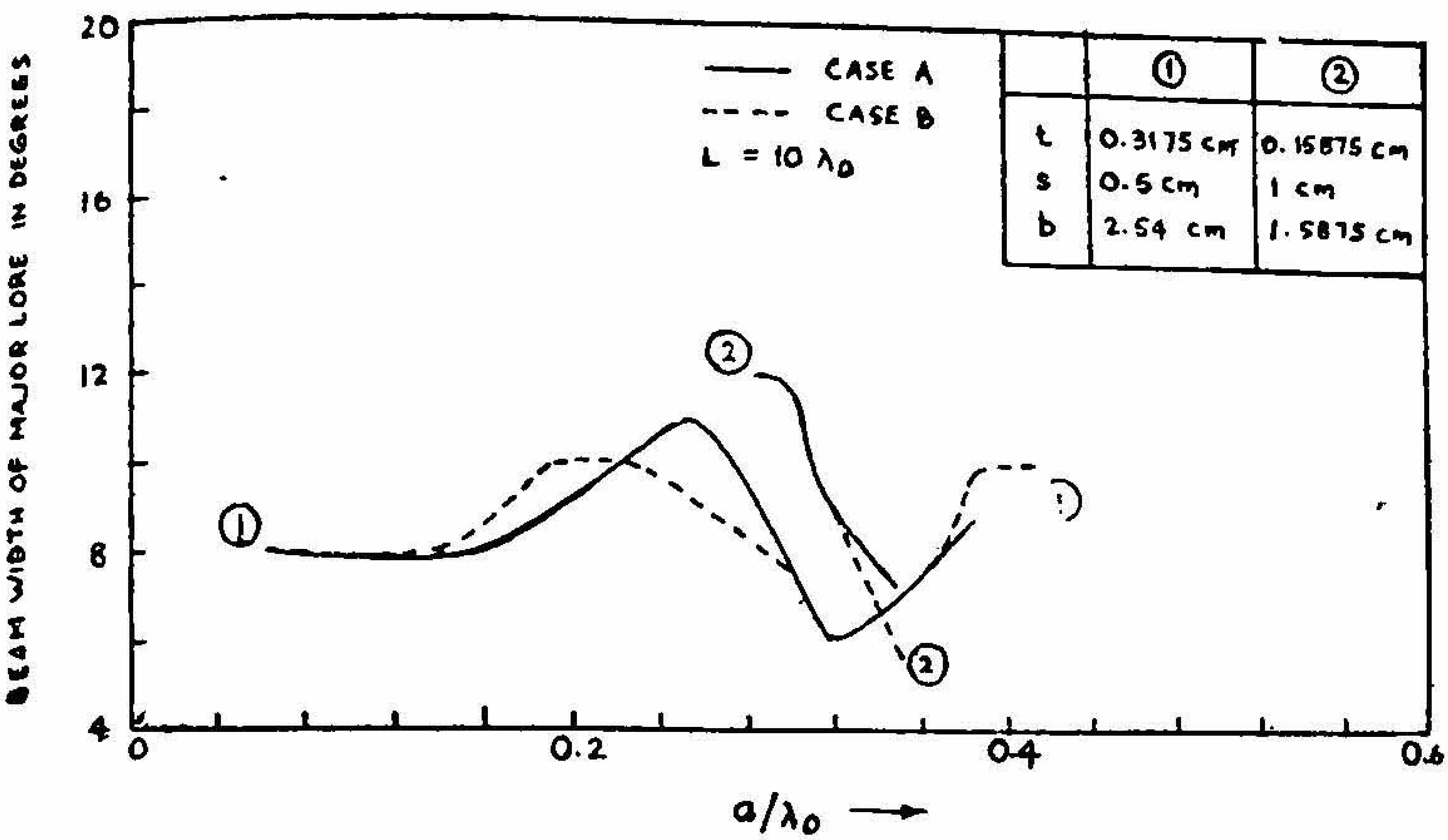

FIG. 23

Beam width of major lobe vs a/λ_0 far corrugated dielectfic rod

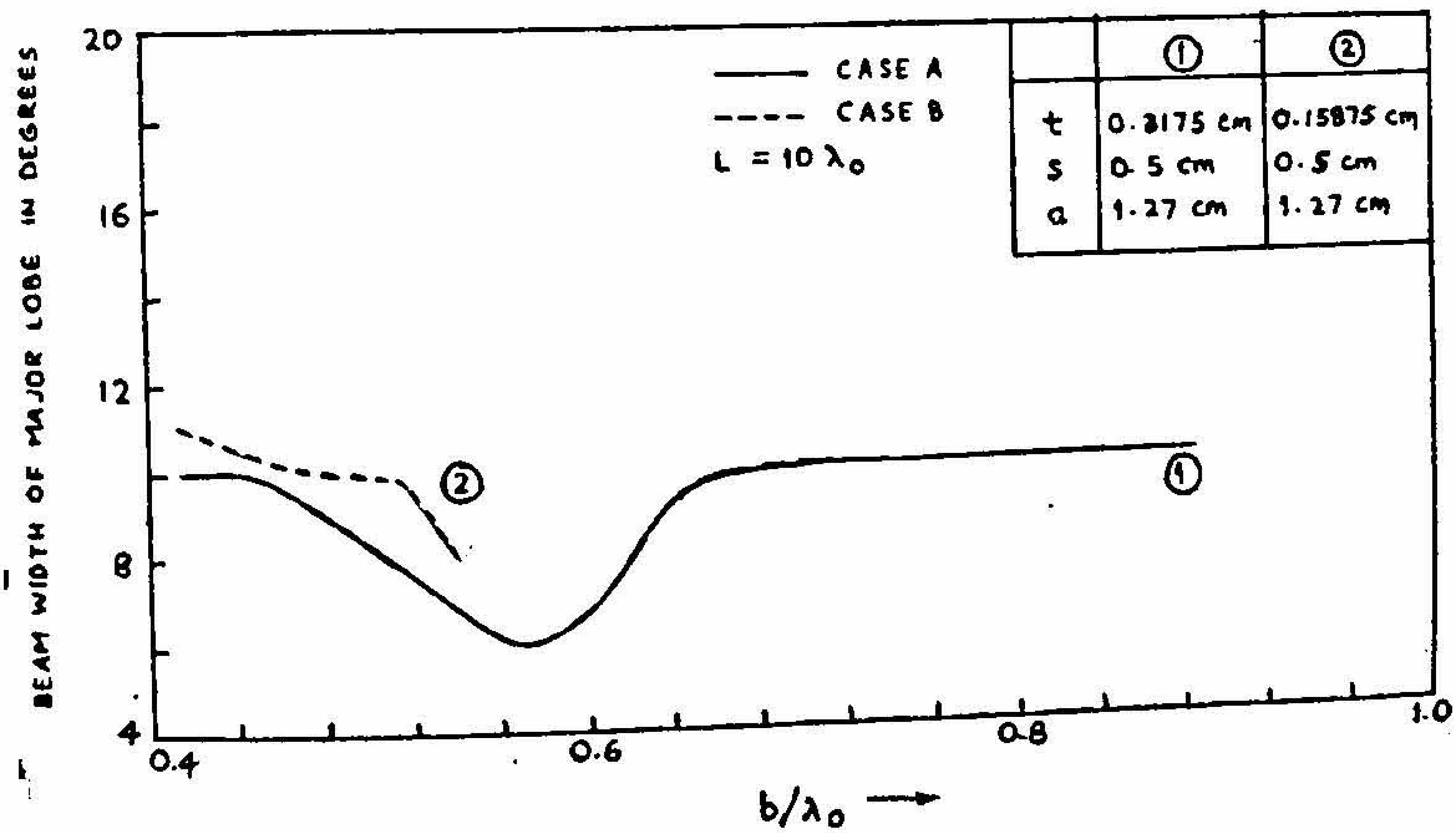

FIG. 24

Beam width of major lobe vs b/λ_0 for corrugated dielectric rod

L = Length of the rod
t = Disc thickness
s = Disc spacing
a = Inner rod radius
b = Disc radius
λ_0 = 3.14 cm.

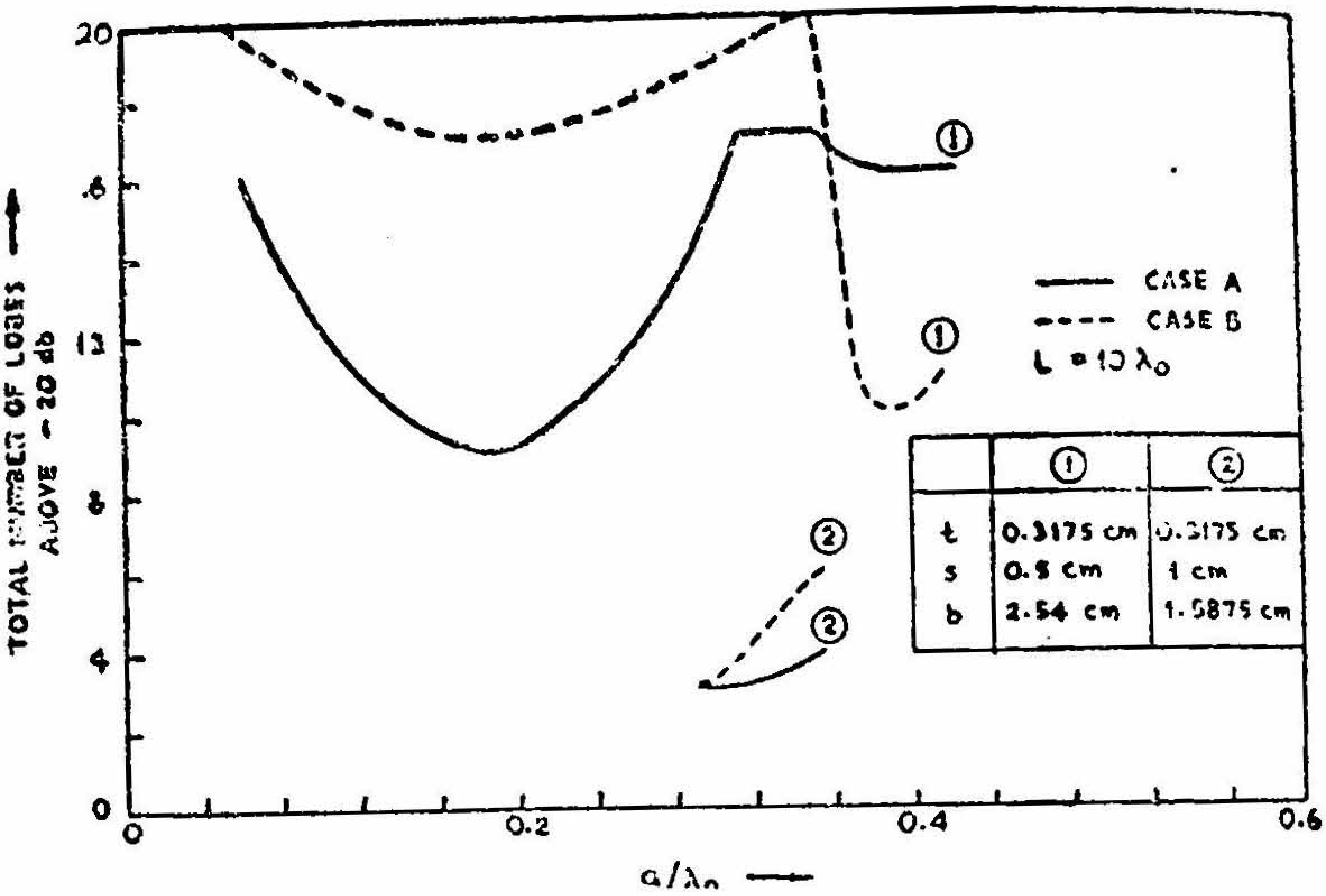

FIG. 25

Number of lobes vs a/λ_0 for corrugated dielectric rod

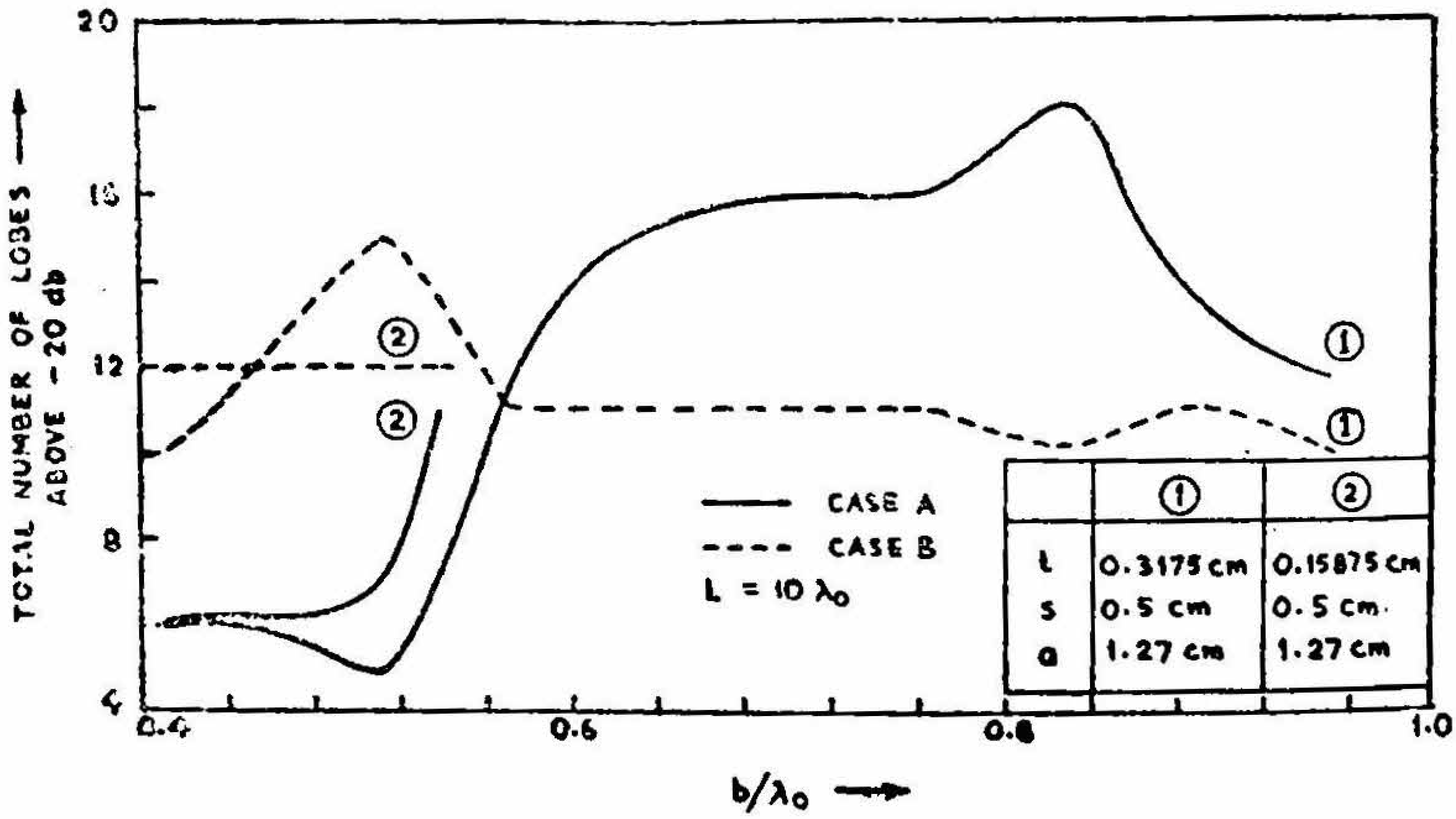

FIG. 26

Number of lobes vs b/λ_0 for corrugated dielectric rod

L - Length of the rod s = Disc spacing b = Disc radius

t = Disc thickness a = Inner rod radius λ_0 = 3.14 cm.

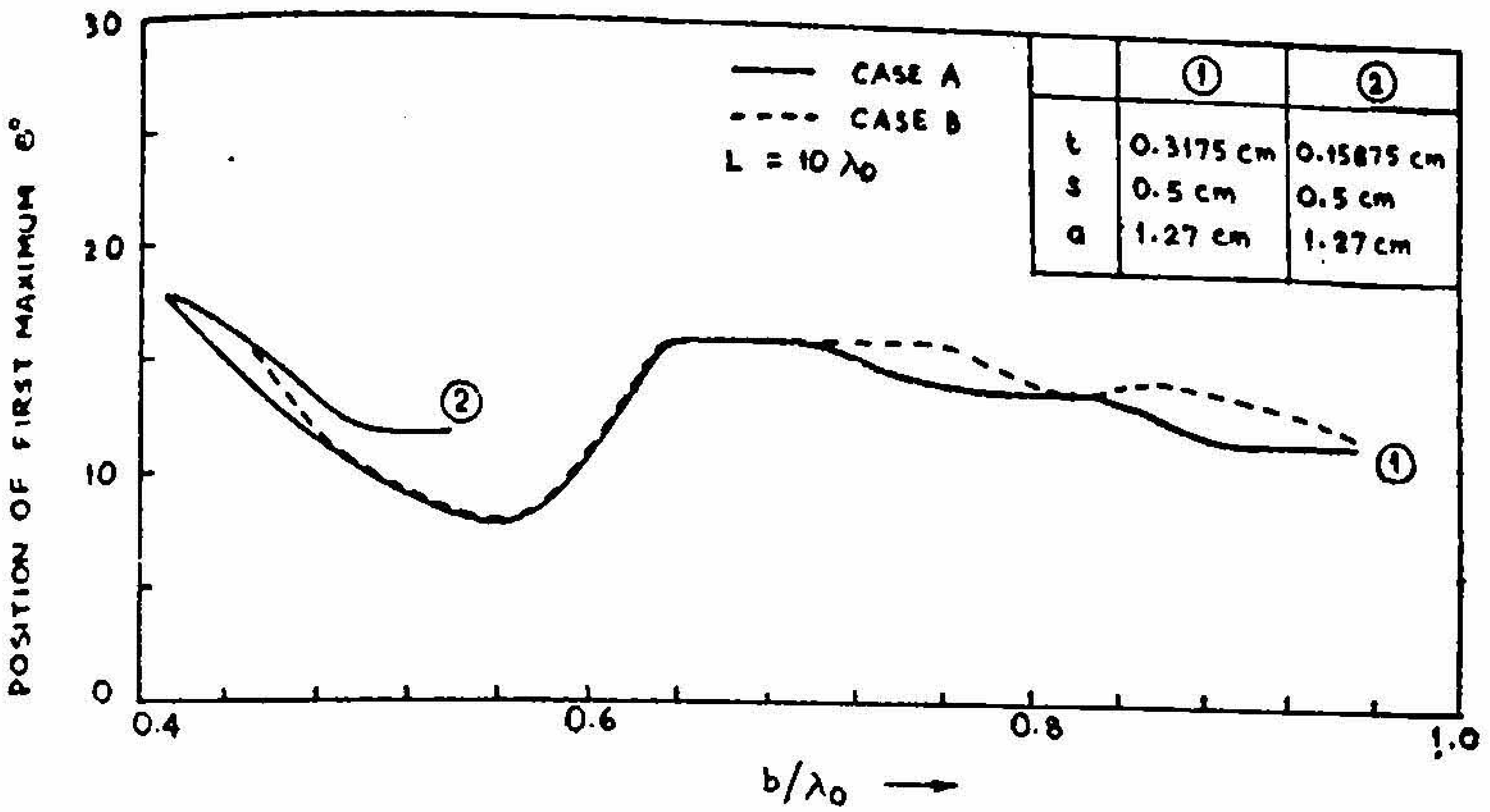

FIG. 27

Position of first maximum vs b/λ_0 for corrugated dielectric rod

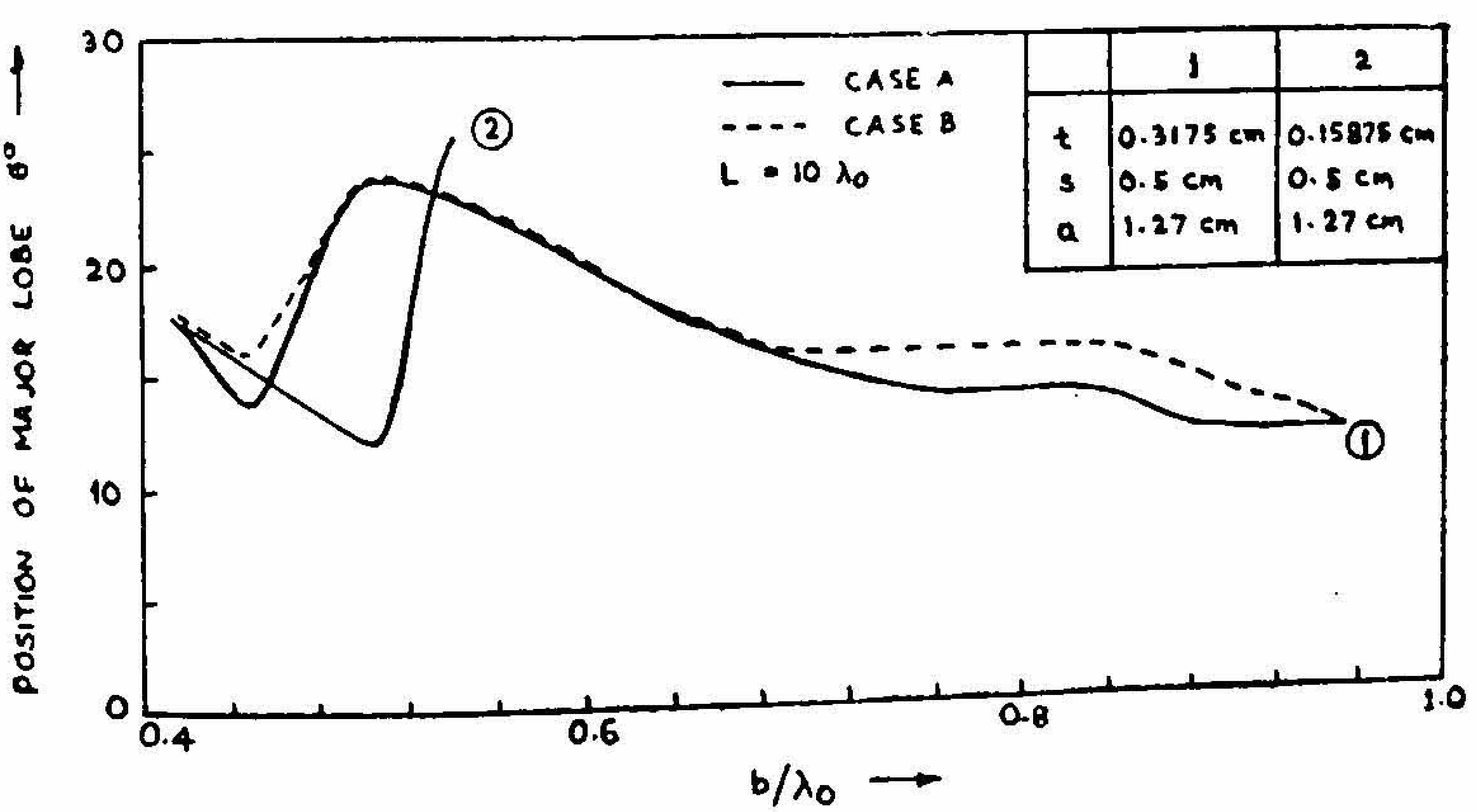

FIG. 28

Position of major lobe vs b/λ_0 for corrugated dielectric rod

L = Length of the rod
t - Disc thickness
s - Disc spacing
a - Inner rod radius
b - Disc radius
λ_0 = 3.14 cm.

where,

$$P_z^i = \frac{1}{2} \operatorname{Re} \int_{\phi'=0}^{2\pi} \int_{\rho=0}^{a} E_{\rho 1} H_{\phi' 1}^{*} \rho \, d\rho \, d\phi' \tag{33a}$$

and

$$P_z^0 - \frac{1}{2} \operatorname{Re} \int_{\phi'-0}^{2\pi} \int_{\rho=a}^{\infty} E_{\rho 2} H_{\phi' 2}^{*} \rho \, d\rho \, d\phi' \tag{33b}$$

which after substitution of appropriate components and integration reduce to

$$\mathrm{P}_z^i = \frac{1}{2} \operatorname{Re}\left(\frac{B^2 (k'_1)^2 \beta}{\omega \epsilon_1} \int_0^{2\pi} \int_0^{a} \rho \, \mathrm{J}_1^2 (k'_1 \rho) \, d\rho \, d\phi' \right)$$

$$= \frac{\pi B^2 \beta a^2 (k'_1)^2}{2 \omega \epsilon_0 \epsilon_{r1}} \left\{ \{ \mathrm{J}_0(k'_1 a)\}^2 + \{ \mathrm{J}_1(k'_1 a)\}^2 - \left(\frac{2 \mathrm{J}_0(k'_1 a) \mathrm{J}_1(k'_1 a)}{k'_1 a} \right) \right\} \tag{34}$$

and

$$\mathrm{P}_z^0 = \frac{1}{2} \operatorname{Re} \frac{\pi D^2 \beta k'_2 (k'_2)^*}{\omega \epsilon_0} \int_a^{\infty} \rho \, \mathrm{H}_1^{(1)}(k'_2) \, \mathrm{H}_1^{(2)}(k_2'^{*}) \, d\rho$$

$$= \operatorname{Re} \left\{ \frac{\pi D^3 (k'_2)^2 \beta a^2}{2 \omega \epsilon_0} [\mathrm{H}_0^{(1)}(k'_2 a)]^2 + [\mathrm{H}_1^{(1)}(k'_2 a)]^2 - \left(\frac{2 \mathrm{H}_0^{(1)}(k'_2 a) \mathrm{H}_1^{(1)}(k'_2 a)}{k'_2 a} \right) \right\} \tag{35}$$

The constants B and D are related by boundary conditions as follows

$$D = \frac{B}{\epsilon_{r1}} (k'_1 / k'_2)^2 \frac{\mathrm{J}_0(k'_1 a)}{\mathrm{H}_0^{(1)}(k'_2 a)} \tag{36}$$

The total power flow in the z-direction is, therefore given by

$$\mathrm{P}_{zt} = \left(\frac{\pi B^2 \beta a^2 (k'_1)^2}{2 \omega \epsilon_0 \epsilon_{r1}} \right) \Bigg[\left\{ \{ \mathrm{J}_0(k'_1 a)\}^2 + \{ \mathrm{J}_1(k'_1 a)\}^2 - \left(\frac{2 \mathrm{J}_0(k'_1 a) \mathrm{J}_1(k'_1 a)}{k'_1 a} \right) \right.$$

$$+ \left\{ \frac{1}{\epsilon_{r1}} \left(\frac{k'_1}{k'_2} \right)^2 \left(\frac{\mathrm{J}_0(k'_1 a)}{\mathrm{H}_0^{(1)}(k'_2 a)} \right)^2 \right\} \Big\{ [\mathrm{H}_0^{(1)}(k'_2 a)]^2 + [\mathrm{H}_1^{(1)}(k'_2 a)]^2$$

$$\left. - \left(\frac{2 \mathrm{H}_0^{(1)}(k'_2 a) \mathrm{H}_1^{(1)}(k'_2 a)}{k'_2 a} \right) \Big\} \right\} \Bigg] \tag{37}$$

5.1.2 *Radiated Field*

The radiated field at P (r, θ, ϕ) due to radiation from the surfaces only is

$$E_{PS} = B \cdot \left\{ \frac{1}{2r} \left(\frac{\mu_0}{\epsilon_0} \right)^{1/2} a\, k\, k'_1\, J_1(k'_1 a) \right\} \left(L \frac{\sin \frac{1}{2} L (\beta - k \cos \theta)}{\frac{1}{2} L (\beta - k \cos \theta)} \{J_0(ka \sin \theta)\} \sin \theta - \frac{k'_1 J_0(k'_1 a)}{\epsilon_{r1}\, k\, J_1(k'_1 a)} J_1(ka \sin \theta) \right) \quad [38]$$

The radiated field at P (r, θ, ϕ) due to radiation from the surface and free end of the rod is calculated from the expression

$$|E_P| = [E_{PS}^2 + E_{Pe}^2 + 2\, E_{PS}\, E_{Pe} \sin (L/2)\, (\beta - k \cos \theta)]^{1/2} \quad [39]$$

where,

$$E_{Pe} = B \left\{ \frac{1}{2r} \left(\frac{\mu_0}{\epsilon_0} \right)^{1/2} a\, k\, k'_1 J'_1 a) \left(k \cos \theta + \frac{\beta}{\epsilon_{r1}} \right) \times \right.$$
$$\left. \times \left(\frac{J_0(ka \sin \theta) \sin \theta - [k'_1 J_0(k'_1 a)/k J_1(k'_1 a)]\, k'_1 J_1(ka \sin \theta)}{(k'_1)^2 - (k \sin \theta)^2} \right) \right\} \quad [40]$$

5.1.3 *Numerical Computation of Gain of Uniform Dielectric Rod*

The gain is computed from the following relation [41] and equations [37] and [39].

$$= \frac{\gamma' \, |E_P|^2/2\, \eta_0}{P_{zt}/4} \quad [41]$$

where, $\eta_0 = (\mu_0/\epsilon_0)^{1/2}$

r = distance of P (r, θ, ϕ) from the origin

$|E_P|^2$ = maximum value of the square of the radiated field

Variation of gain with respect to L/λ_0 and a/λ_0 is shown in Figs. 29 and 30 respectively

5.2 *Gain of corrugated Dielectrtc Rod*

The gain calculations are made in a similar way to that of uniform rod.

5.2.1 *Power Flow*

The total power flow P_{zt} along the corrugated rod is given by the relation

$$P_{zt} = P_z^{(1)} + P_z^{(2)} + P_z^{(3)} \quad [42]$$

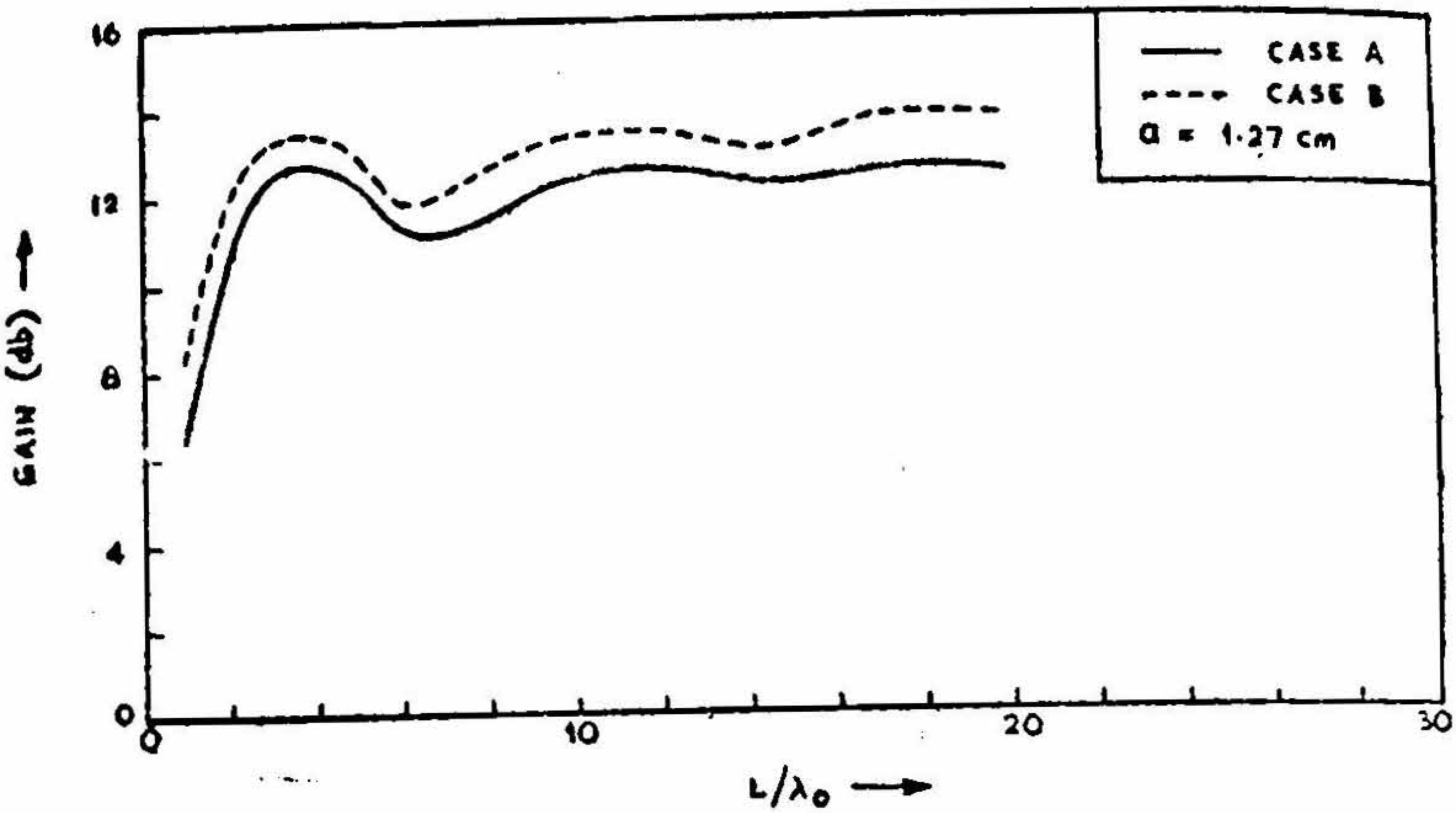

FIG. 29

Variation of gain with L/λ_0 for uniform dielectric rod

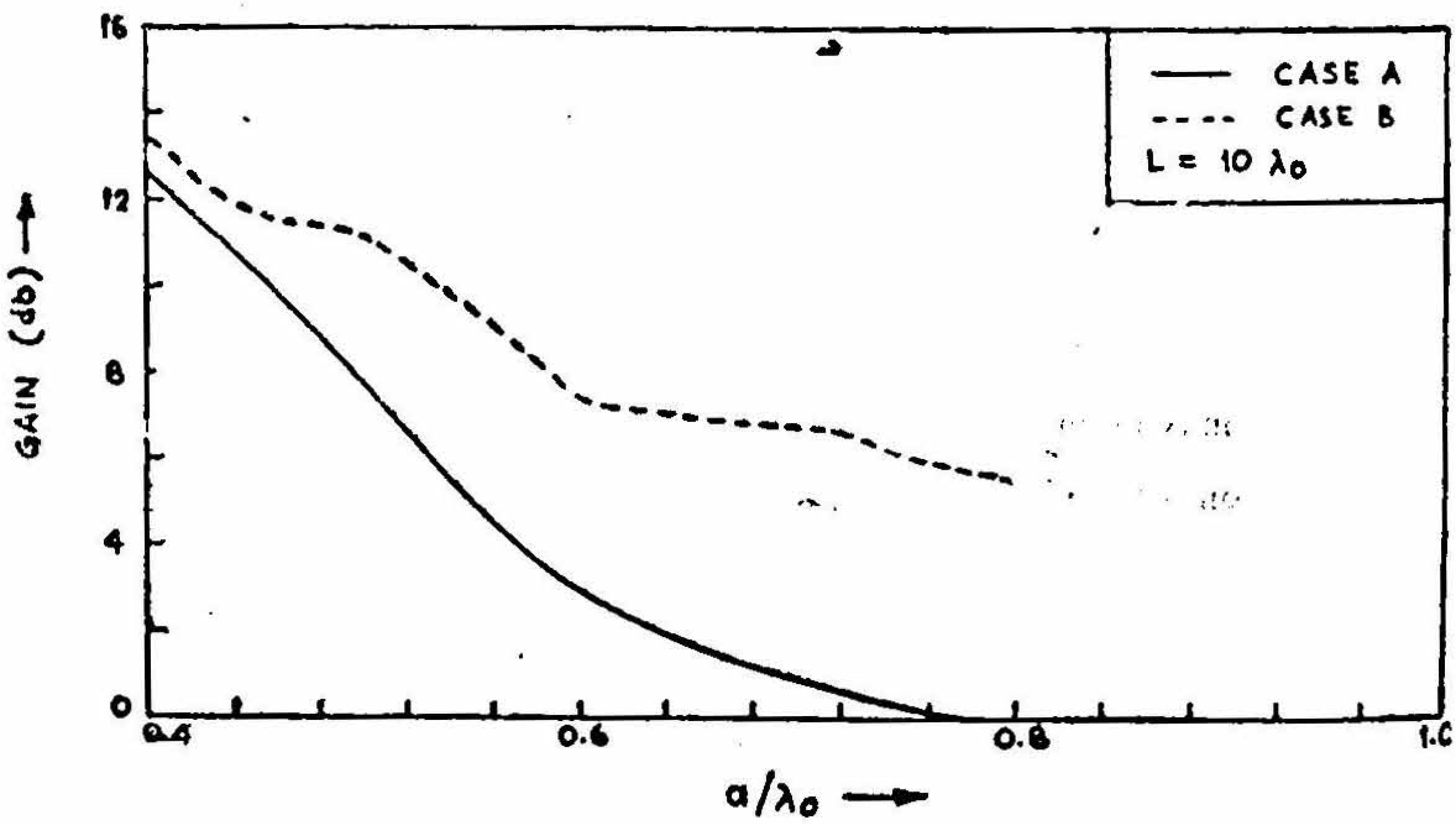

FIG. 30

Variation of gain with a/λ_0 for uniform dielectric rod

l = Length of the rod a = Radius of the rod λ_0 = 3.14 cm where, the power flow in the three regions $P_z^{(1)}$, $P_z^{(2)}$ and $P_z^{(3)}$ are given respectively by the following relations

$$P_z^{(1)}=\frac{1}{2}\ \mathrm{Re}\int_{\rho=0}^{a}\int_{\phi'=0}^{2\pi} E_{\rho 1}\, H^*_{\phi' 1}\, \rho\, d\rho\, d\phi' \tag{43}$$

$$P_z^{(2)}=\frac{1}{2}\ \mathrm{Re}\int_{\rho=a}^{b}\int_{\phi'=0}^{2\pi} E_{\rho 2}\, H^*_{\phi' 2}\, \rho\, d\rho\, d\phi' \tag{44}$$

$$P_z^{(3)}=\frac{1}{2}\ \mathrm{Re}\int_{\phi=b}^{\infty}\int_{\phi'=0}^{2\pi} E_{\rho 3}\, H^*_{\phi' 3}\, \rho\, d\rho\, d\phi' \tag{45}$$

which after substitution of appropriate field components and integrations become

$$P_z^{(1)}=\frac{\pi\omega\epsilon_1\,\beta\, a^2}{2\, k_1^2}A_1^2\left\{\{\mathrm{J}_0(k_1a)\}^2+\{\mathrm{J}_1k_1a)\}^2-\left(\frac{2\,\mathrm{J}_0(k_1a)\,\mathrm{J}_1(k_1a)}{k_1a}\right)\right\} \tag{46}$$

$$\begin{aligned}
P_z^{(2)}=&\left(\frac{\pi\omega\epsilon_2\beta}{2\,k_2^2}\right)\Bigg[\{b^2A_2^2\}\left\{[\mathrm{J}_0(k_2b)]^2+[\mathrm{J}_1(k_2b)]^2-\left(\frac{2\mathrm{J}_0(k_2b)\,\mathrm{J}_1(k_2b)}{k_2b}\right)\right\}\\
&+\{A_3^2\,b^2\}\left\{[Y_0(k_2b)]^2+[Y_1(k_2b)]^2-\left(\frac{2\,Y_0(k_2b)\,Y_1(k_2b)}{k_2b}\right)\right\}\\
&+\left(\frac{A_2A_3b^2}{2}\right)\{2\,\mathrm{J}_1(k_2b)\,Y_1(k_2b)-\mathrm{J}_0(k_2b)\,Y_2(k_2b)-\mathrm{J}_2(k_2b)\,Y_0(k_2b)\}\\
&-\{a^2A_2^2\}[\,\mathrm{J}_0(k_2a)\,]^2+[\,\mathrm{J}_1(k_2a)\,]^2-\left(\frac{2\,\mathrm{J}_0(k_2a)\,\mathrm{J}_1(k_2a)}{k_2b}\right)\\
&-\{a^2A_3^2\}[Y_0(k_2a)]^2+[Y_1(k_2a)]^2-\left(\frac{2Y_0(k_2a)\,Y_1(k_2a)}{k_2a}\right)\\
&-\left(\frac{a^2A_2A_3}{2}\right)\{2\,\mathrm{J}_1(k_2a)\,Y_1(k_2a)-\mathrm{J}_0(k_2a)\,Y_2(k_2a)-J_2(k_2a)\,Y_0(k_2a)\}\Bigg]
\end{aligned} \tag{47}$$

$$P_z^{(3)}=\frac{\pi\omega\epsilon_0\,b^2\beta}{2\,k_3^2}A_4^2\left\{\{H_0^{(1)}(k_3b)\}^2+\{H_1^{(1)}(k_3b)\}^2-\left(\frac{2\,H_0^{(1)}(k_3b)\,H_1^{(1)}(k_3b)}{k_3b}\right)\right\} \tag{48}$$

A_3 and A_4 are expressed in terms of A_2 by using the boundry conditions at $\rho=a$ and $\rho=b$

The total power flow is

$$P_{zt}=\frac{\pi\,\beta\,k A_2^2}{2\eta_0}\Bigg[\left(\frac{a^2\epsilon_{r1}}{k_1^2}C_2^2\right)\left\{[J_0(k_1a)]^2+[J_1(k_1a)]^2-\left(\frac{2J_0(k_1a)\,J_1(k_1a)}{k_1a}\right)\right\}$$

$$+\left(\frac{b^2\epsilon_{r2}}{k_2^2}\right)\left\{[J_0(k_2b)]^2+[J_1(k_2b)]^2-\left(\frac{2\,J_0(k_2b)\,J_1(k_2b)}{k_2b}\right)\right\}$$

$$+\{b^2C_1^2\}\left\{[Y_0(k_2b)]^2+[Y_1(k_2b)]^2-\left(\frac{2\,Y_0(k_2b)\,Y_1(k_2b)}{k_2b}\right)\right\}$$

$$+\{b^2C_1\}\Bigg(J_1(k_2b)\,Y_1(k_2b)-\frac{J_0(k_2b)\,Y_1(k_2b)}{k_2b}+J_0(k_2b)\,Y_0(k_2b)$$

$$-\frac{Y_0(k_2b)\,J_1(k_2b)}{k_2b}\Bigg)-\{a^2\}\left\{[J_0(k_2a)]^2+[J_1(k_2a)]^2-\left(\frac{2\,J_0(k_2a)\,J_1(k_2a)}{k_2a}\right)\right\}$$

$$-\{a^2C_1^2\}\left\{[Y_0(k_2a)]^2+[Y_1(k_2a)]^2-\left(\frac{2\,Y_0(k_2a)\,Y_1(k_2a)}{k_2a}\right)\right\}$$

$$-\{a^2C_1\}\Bigg\{J_1(k_2a)\,Y_1(k_2a)-\frac{J_0(k_2a)\,J_1(k_2a)}{k_2a}$$

$$+J_0(k_2a)\,Y_0(k_2a)-\frac{Y_0(k_2a)\,J_1(k_2a)}{k_2a}\Bigg\}$$

$$+\left(\frac{b^2C_3^2}{k_3^2}\right)\left\{[H_0^{(1)}(k_3b)]^2+[H_1^{(1)}(k_3b)]^2-\left(\frac{2\,H_0^{(1)}(k_3b)\,H_1^{(1)}(k_3b)}{k_3b}\right)\right\}\Bigg] \qquad [49]$$

where,

$$C_1=\frac{[k\epsilon_{r2}\,C/k_2]\,J_1(k_2b)-J_0(k_2b)}{Y_0(k_2b)-[k_{r2}/k_2]\,C\,Y_1(k_2b)} \qquad [49a]$$

$$C_2=\frac{J_0(k_2a)+C_1\,Y_0(k_2a)}{J_0(k_1a)} \qquad [49b]$$

$$C_3=\frac{J_0(k_2b)+C_1\,Y_0(k_2b)}{H_0^{(1)}(k_3b)} \qquad [49c]$$

$$C=\frac{k_3}{k}\,\frac{H_0^{(1)}(k_3b)}{H_1^{(1)}(k_3b)} \qquad [49d]$$

5.2.2 *Radiated Field*

Case A: The radiated field at P (r, θ, ϕ) is obtained from equation [28].

$$E_{P_c} = \left[\left\{ \frac{L\, b\, k^2 \epsilon_{r2}}{k_2} A_2 \right\} \{ J_1(k_2 b) + C_1\, Y_1(k_2 b) \} \right] \times$$

$$[\{ J_0(kb \sin\theta) - C\, J_1(kb \sin\theta) \sin\theta \}] \left(\frac{\sin \frac{1}{2}L\,(\beta - k\cos\theta)}{\frac{1}{2}L\,(\beta - k\cos\theta)} \right) \quad [50]$$

Case B: The radiation field at P is obtained from equation [32].

$$|E_P| = [E_{PS}^2 + E_{Pe}^2 + 2\, E_{PS}\, E_{Pe} \sin(L/2)(\beta - k\cos\theta]^{1/2} \quad [51]$$

where,

$$E_{Pe} = \left(\frac{C_2 ka}{k_1} (k\epsilon_{r1} \cos\theta + \beta) \right) \left(\frac{k_1 J_1(ka \sin\theta) J_0(k_1 a) - (k \sin\theta) J_1(k_1 a) J_0(ka \sin\theta)}{k_1^2 - (k\sin\theta)^2} \right)$$

5.2.3 *Numerical Computation of Gain of Corrugated Dielectric Rod*

The gain of corrugated dielectric rods computed with the aid of equations [28], [32], [41] and [49] for the following combinations of structure parameters

(i) $t = 0.15875$ cm, $a = 0.9525$ cm, $b = 1.5875$ cm
(ii) $t = 0.15875$ cm, $a = 0.9525$ cm, $b = 1.905$ cm

and as function of s/λ_0 is shown in Figures [31] and [32].

The variation of gain as a function of a/λ_0 for the following combinations of the structure parameters

(i) $t = 0.3175$ cm, $s = 0.5$ cm, $b = 2.54$ cm.
(ii) $t = 0.15875$ cm, $s = 1$ cm, $b = 1.5875$ cm.

is shown in Fig. 33.

The variation of gain computed as a function of b/λ_0 for the following combination of structure parameters is shown in Fig. 34.

(i) $t = 0.3175$ cm, $s = 0.5$ cm, $a = 1.27$ cm.
(ii) $t = 0.15875$ cm, $s = 0.5$ cm, $a = 1.27$ cm.

The following remarks regarding gain may be interesting

(i) The gain of uniform dielectric rod decreases with increasing diameter. For larger diameters, there is significant difference in gain in the two Cases A and B, which indicates that free end radiation plays an important role, especially, in the case of rod of larger diameter.

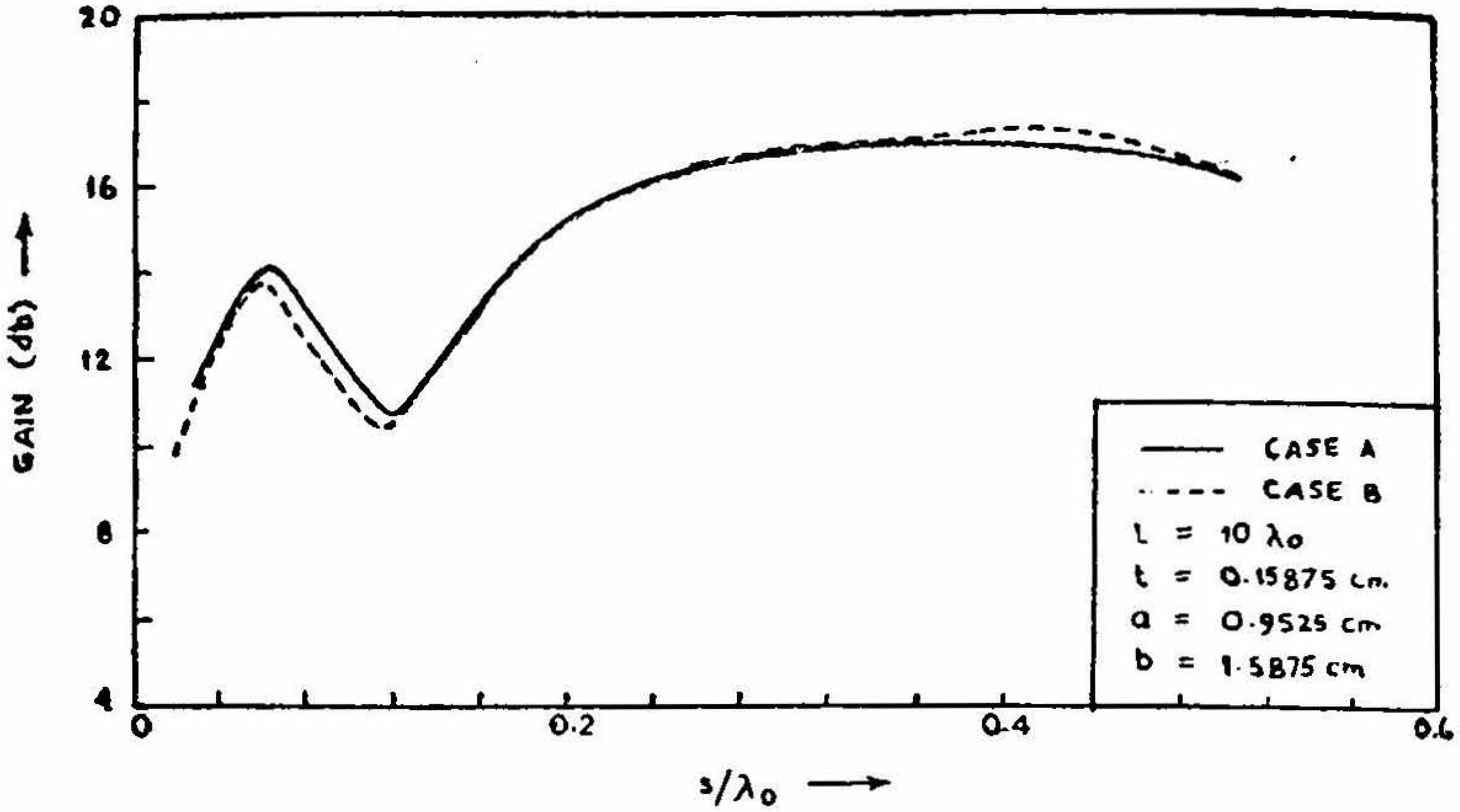

FIG. 31

Variation of gain with s/λ_0 for corrugated dielectric rod

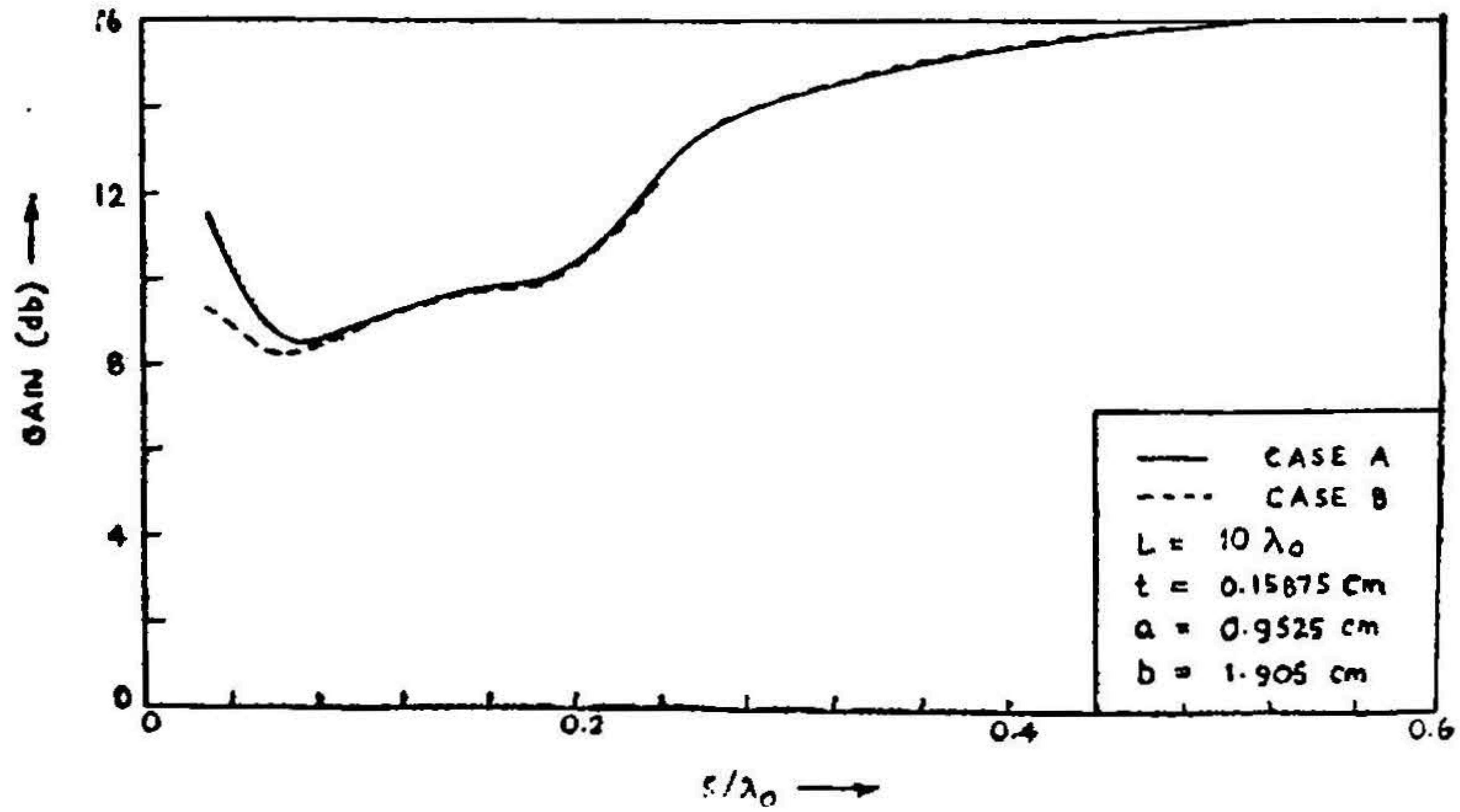

FIG. 32

Variation of gain with s/λ_0 for corrugated dielectric rod

L = Length of the rod	s = Disc spacing	b = Disc radius
t = Disc thickness	a = Inner rod radius	λ_0 = 3.14 cm.

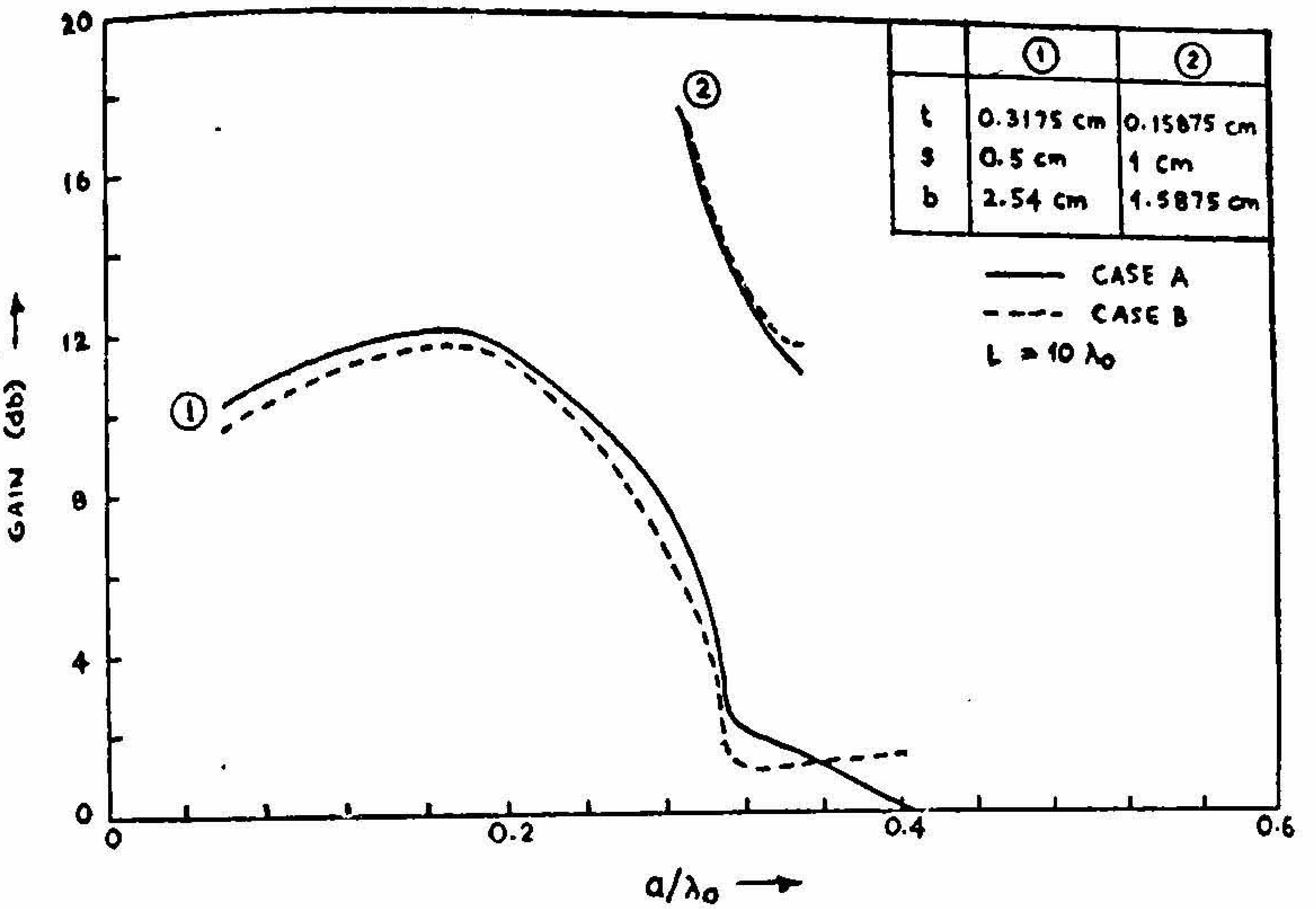

FIG. 33

Variation of gain with a/λ for corrugated dielectric rod

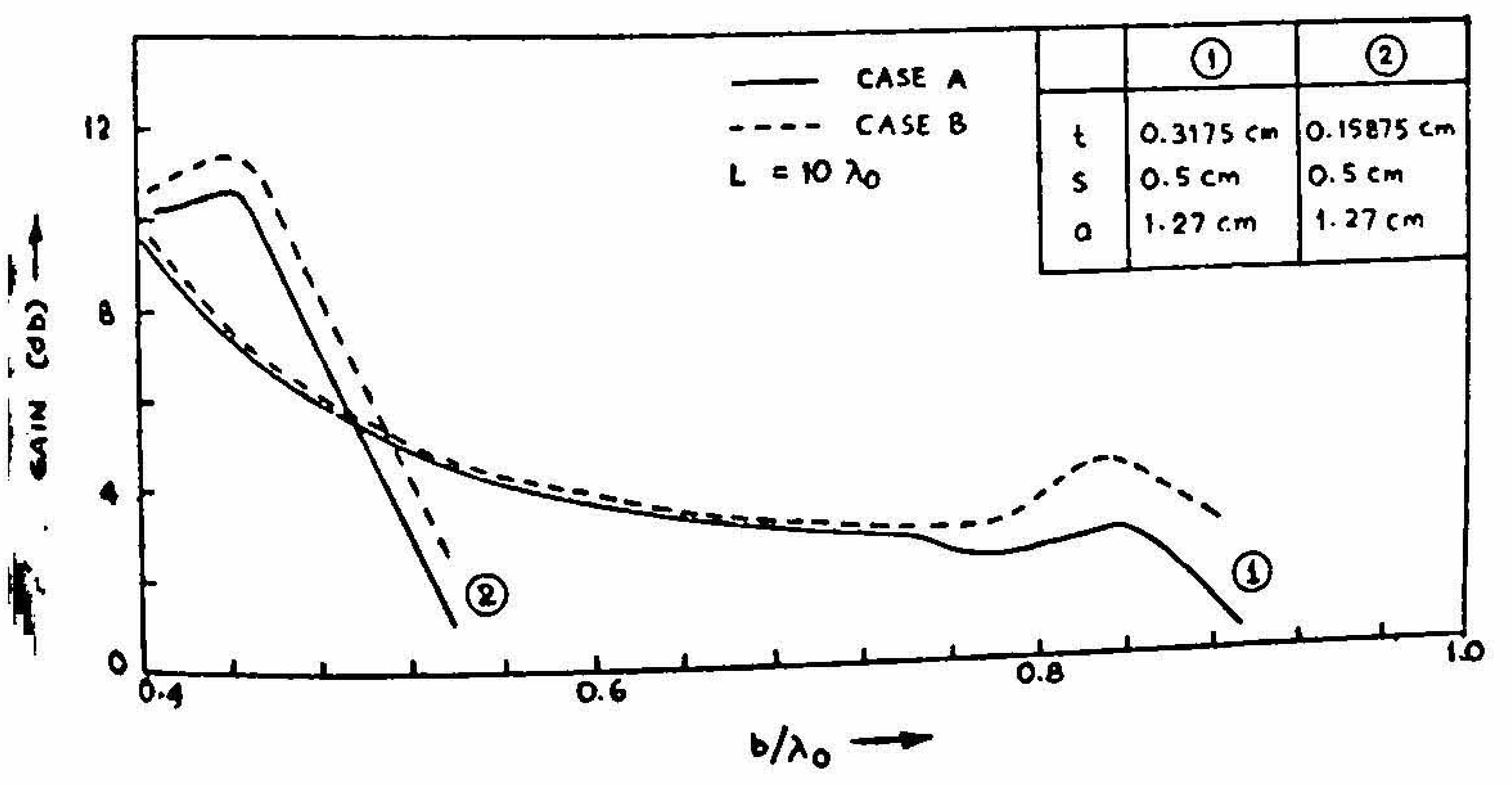

FIG. 34

Variation of gain with b/λ_0 for corrugated dieletric rod

L = Length of the rod
t = Disc thickness
s = Disc spacing
a = Inner rod radius
b = Disc radius
λ_0 = 3.14 cm.

(ii) The gain of corrugated rods is oscillatory for smaller values of s/λ_0, then increases and finally tends towards a constant value at larger values of s/λ_0.

6. CONCLUSION

(i) In the case of corrugated rods radiation characteristics can be controlled by variation of groove depth and spacing. This gives an advantage over uniform rod as in both the types of aerials the radiation characteristic is a function of the length, diameter and dielectric constant of the rod.

(ii) In case of corrugated rods, the factors '*a*' and '*b*' seem to play more important role in controlling radiation pattern than other factors, viz., '*t*' and '*s*'.

(iii) It is possible to achieve the reduction of the number and intensities of minor lobes by a proper selection of the combinations of structure parameters.

7. ACKNOWLEDGMENT

The authors are grateful to Dr. S. Dhawan, Director of the Indian Institute of Science for permission to accept the work the scheme and giving necessary facilities. The authors also expresses their deep gratitude to Dr. James R. Wait, Monitor, Senior Scientist O/T—ITS for support, encouragment and technical advice for this project. They also express their grateful thanks to U. S. Department of Commerce for providing PL—480 fund and to U. G. C., New Delhi for permission to conduct this project and also to N.O.A.A.

8. REFERENCES

1. Muller, G. E. and Tyrell, W. A. .. *B. S. T. J.* 1947, 26, 837.
2. Haliday, D. F. and Kiely, D. G. .. *J. I. E. E.* 1947, 94, 610—618.
3. Chatterjee, (Mrs.) R. and Chatterjee, S. K. .. *J. Indian Inst. Sci.*, 1957, 39. 134.
4. Wikes, G. .. .. *Proc I. R. E.*, 1948, 36, 206—212.
5. Hortou. C. W., Karal F. C. Jr. and Mckinney .. *J. Appl. Pnysics*, 1950, 21, 1279—1283.
6. Chatterjee (Mrs.) R. and Chatterjee. S. K. .. *J. Indlan Inst. Sci.*, 1956, 38, 93.
7. Ramanujam, H. R. and .. Chatterjee (Mrs.) R. .. *J. Indian Inst. Sci.*, 1962 44, 164, 203.
8. Bouix. M. .. .. .. "Contribution a l' etude des Antennas dielectrique" Thesis for the degree of D.e'SS L' university de Paris, 1952.
9. Watson, R. B. and Horton, C. W. .. *J. Appl. Phys.* 1948, 19, 836—837.
10. Brown, J. and Spector, .. *Proc. I. E. E.* 1957 B, 104, 27—34.